Petrogenesis of Glasses and Microlites in Mantle Xenoliths from Baikal-Mongolia Region : a Review

Petrogenesis of Glasses and Microlites in Mantle Xenoliths from Baikal-Mongolia Region: a Review

Konstantin LITASOV *, Viktor SHARYGIN **, Vladimir SIMONOV***,
Vladimir MALKOVETS ****, Hiromitsu TANIGUCHI ****

Key words: mantle xenolith, interstitial glasses, microlites, fluid inclusions, partial melting

Abstract

Petrogenesis of various glasses, microlite assemblages and fluid and melt inclusions in minerals of mantle xenoliths from alkaline volcanics of Baikal-Mongolian region is discussed. Diversity and compositional variations of glasses vary widely and their origin can be addressed to most of previously reported hypotheses. Study of the fluid inclusions indicates that depth of trapping is usually well correlated with the depth of Moho estimated from seismological and petrological data. The density of CO_2 fluid inclusions indicates minimum pressures of their origin of 10-15 kbar.

Glasses from melt inclusions in minerals of Dzhilinda xenoliths (Vitim flied) can represent direct melts formed by in situ partial melting of peridotite at about 10 kbar, the pressure estimated from fluid inclusions, whereas glasses from melt inclusions in minerals of garnet lherzolite of Bereya Quarry (Vitim flied) can represent melts formed at pressures above 15 kbar. The SiO_2 contents of these glasses (51–57 wt.%) are consistent with those of experimental partial melts from low-degree partial melting of peridotite.

Origin of SiO_2-rich (up to 74 wt.%) glasses from harzburgite xenoliths is consistent with experimental study by Shaw *et al.* (1998) indicating that reaction of orthopyroxene with silica-undersaturated melt at ambient pressure results in olivine, clinopyroxene, spinel and intermediate of silicic melt.

We describe unusual clinopyroxene-olivine-sanidine symplectites in high-temperature spinel lherzolites from Burkal locality. Calculated bulk compositions of the symplectites indicate that they can represent breakdown after K-bearing pyroxene solid solution from deep mantle.

1. Introduction

Interstitial glasses in mantle xenoliths and fluid or melt inclusions in their minerals are an important source of petrological information about silicate melts potentially in equilibrium with mantle assemblages and critical for understanding metasomatic

* Institute of Mineralogy, Petrology and Economic Geology, Faculty of Science, Tohoku University
** United Institute of Geology, Geophysics and Mineralogy, Novosibirsk, Russia
*** GEMOC National Key Center, Department of Earth and Planetary Sciences, Macquarie University, Sydney, Australia
**** Center for Northeastern Asian Studies, Tohoku University

processes in sublithospheric mantle. Interstitial glasses have been reported from many mantle xenoliths hosted by alkaline basaltic magmas from suboceanic tectonic settings (e.g. Schiano *et al.*, 1995; Wulff-Pedersen *et al.*, 1996; 1999; Newmann and Wulff-Pedersen, 1997; Coltorti *et al.*, 1999). They are more rarely originated from rift-related continental basaltic rocks (e.g. Edgar *et al.*, 1989; Ionov *et al.*, 1994; Zingrebbe and Foley, 1995). The glasses have a wide range of compositions and textural relations: they form interstitial veins, veinlets, films, and larger blebs, patches, and melt pockets. Sometimes they can occupy as much as few volume percent of host xenoliths. Draper and Green (1997) summarized many of published glass compositions and suggest they falling into every compositional field except picrobasalts in the alkali versus silica classification diagram of LeMaitre (1989), varying in SiO_2 content in range of 42–74 wt.%. Total alkali content (Na_2O+K_2O) can be up to 17 wt.%.

Information about small-scale metasomatism and glasses from Baikal and Mongolia xenoliths are rather restricted (Dobretsov *et al.*, 1992; Schiano and Clocchiatti, 1994; Schiano *et al.*, 1994; Ionov *et al.*, 1994; 1995; Sharygin *et al.*, 1998; Litasov *et al.*, 1999a; 2002; 2003a,b) compared to other world localities. Recently Litasov and Taniguchi (2002) made comprehensive review of mantle xenoliths from Baikal-Mongolia region, and provided many photographs of xenoliths microstructures including those for some interstitial glasses and melt pockets. However they did not pay much attention for studying chemical composition and petrogenesis of the glasses and microlites. Meanwhile, Baikal-Mongolia xenoliths often contain glasses, melt pockets, and melt and fluid inclusions in minerals and as well as they have great compositional variations they can be very interesting for petrological purposes. In this study we review different types of xenolith glasses from Late Cenozoic alkaline basalts of several volcanic fields in Baikal-Mongolia region. The main goals of this work are: (1) describe diversity of glasses trapped in the xenoliths; (2) specify depths of entrapment using T-P-estimations of associated melt and fluid inclusions and T-P data for host xenoliths; (3) show some of glasses can be related to small-degree partial melting of lithospheric mantle up to garnet stability depth; and (4) discuss the similarity and distinction between glasses related to partial melting and reaction with metasomatic melt/fluid in the depth and those formed by infiltration of host magma during the entrainment to the surface.

2. Analytical methods

Microthermometric methods were used to determine entrapment pressures, temperatures, and compositions of melt and fluid inclusions (Ermakov and Dolgov, 1979; Roedder, 1984). Samples were studied in the double-polished thinsections (thickness near 100 μm). We used heating and cooling stages of original construction mounted on a petrographic microscope by the method described in Sobolev and Slutsky (1984) and Simonov (1993). The accuracy of the measurements was within $\pm$5℃ above 1000℃ and $\pm$0.1℃ below 0℃ (Simonov, 1993). Experiments with melt and fluid inclusions were carried out in the United Institute of Geology, Geophysics and Mineralogy RAS (Novosibirsk, Russia) and Tohoku University (Sendai, Japan). Homogenization temperatures and density of CO_2 were determined during freezing experiments, while homogenization temperatures of melt inclusions were determined during heating experiments. Heating experiments were conducted up to temperature of

homogenization, corresponding to the final melting of the enclosed solid phases. The samples were then quenched and polished for electron microprobe analyses. Combining the data on density of CO_2-inclusions and homogenization temperatures of associated melt inclusions we estimated the minimum pressure of inclusion trapping using equation of state of CO_2. Isochors from Bottinga and Richet (1981) were used for this purpose.

Minerals and glasses were analyzed in polished thin sections and mounts for major elements using JEOL Superprob microanalyzer (JXA-8800) in the Institute of Mineralogy, Petrology and Economic Geology of Tohoku University in Sendai, Japan and Camebax Micro microanalyzer in the United Institute of Geology, Geophysics and Mineralogy in Novosibirsk, Russia. Analyses were run with 15-20 keV acceleration voltages, 10-40 nA sample current, and 1-10 mm beam size. Oxides and natural and synthetic minerals were used as standards. Matrix corrections were performed by the ZAF-procedure.

3. Geological position and locations of volcanic rocks

Formation of Late Cenozoic alkaline basalts in the Baikal rift and adjacent area of Mongolia and development of Baikal Lake and surrounding sedimentary depressions was connected with rifting processes and mantle plume upwelling near south boundary of the Siberian Craton (Logatchev, 1993; Delvaux *et al*, 1997; Litasov and Taniguchi, 2002). Several stages of Cenozoic volcanic activity can be distinguished using age determinations (Rasskazov, 1993; 1994): (1) Early Paleogene (65-55 Ma); (2) Late Oligocene (30-20 Ma); (3) Middle-Late Miocene (15-5 Ma); and (4) Plio-Pleistocene (3.5-0 Ma). Almost all volcanic fields have several eruption stages and have the Pliocene-Quaternary volcanic cones and valley lava flows. Abundant volcanic field are especially distributed near south edge of Baikal Lake, where some authors propose "South-Baikal hot spot" (e.g. Yarmolyuk *et al.*, 1990; Grachev, 1998).

In the present study we consider glasses and microlites from mantle xenoliths of several major volcanic fields (see Fig.3 in Litasov and Taniguchi, 2002): (1) Oka (East Sayan); (2) Bartoy; (3) Vitim; (4) Udokan; (5) Burkal (Khentey); (6) Shavaryn-Tsaram (Taryat depression, Hangai). In turn, in the Vitim and Udokan volcanic fields we studied several xenolith suites. Chemical compositions and ages of selected host volcanic rocks from different areas after Litasov and Taniguchi (2002) are presented in Table 1. In the Vitim volcanic field most of xenolith-bearing basaltic lavas occur within the Bereya area in the eastern Vitim field. For the present study we selected peridotite xenoliths from (1) Miocene (16 Ma) picrobasalt of Bereya Quarry, and Plio-Pleistocene (2-0.8 Ma) basanites of (2) Dzhilinda River; (3) Bulykhta Brook, and (4) Kandidushka volcano (see Fig.6 in Litasov and Taniguchi, 2002). In the Udokan volcanic field we studied mantle xenoliths from (1) Miocene (14 Ma) melanephelinites of Ingamakit, Munduzhyak and Nizhnii Lurbun volcanoes and Pliocene (3-4 Ma) basanites of (2) Neozhidany volcano and (3) Kuas location.

4. Summary of primary mineralogy of host xenoliths

Alkaline basalts are host for the mantle xenoliths, whereas xenoliths themselves are host for the interstitial glasses and melt pockets bearing with the microlites. Most of studied xenoliths are presented by metasomatized spinel lherzolites, containing minor amphibole or phlogopite, or melt pockets and interstitial glasses. Petrography and

xenolith systematization are presented in Table 2 and were considered in details by Litasov and Taniguchi (2002). Table 2 includes also T-estimations by Brey and Kohler (1990) thermometers and reference numbers for mineral compositions from appendix 3 in Litasov and Taniguchi (2002). Compositions of primary minerals from newly described xenoliths are presented in Table 3.

Xenoliths from the Pliocene basanites of the Vitim field include various garnet-spinel and spinel peridotites and pyroxenites (Litasov and Litasov, 1999; Litasov *et al.*, 2000a,b; Litasov and Taniguchi, 2002). Peridotite xenoliths from Dzhilinda River can be divided into: (1) high-T garnet and spinel lherzolites (Samples D-51, D-82, D-3F), (2) low-T spinel lherzolites and harzburgites (Sample D-11), (3) low-T titaniferous spinel lherzolites (Samples D-2, DY-8A) (Table 2). Protogranular peridotites of the series 1 represent primitive to moderately depleted mantle from the depths 60-80 km at T (2-pyroxene Brey and Kohler, 1990) =1100-1250℃. Trace element patterns in clinopyroxenes are indicative of low degree partial melting of the primitive mantle. Peridotites of the series 2 correspond to the depths 40-50 km at T=800-900℃. Unique titaniferous peridotites (TiO_2=0.55% in the bulk rock) have a mosaic equigranular texture and are suggested to be a rare type of melt/mantle interaction. Their T-estimations (780-850℃) projected to a geotherm correspond to the uppermost mantle section (35-45 km depth). Peridotite xenoliths from Kandidushka volcano are well correspond to high-T series 1 and low-T series 2 of those from Dzhilinda River and peridotites from Bulykhta rivers are mostly of series 1 of those from Dzhilinda.

The major part of the xenoliths from Miocene picrobasalts is represented by garnet lherzolite (see Ionov *et al.*, 1993). The suite also includes variety of spinel peridotites and garnet and spinel pyroxenites and megacryst assemblage. Textural and compositional features are almost similar for the both garnet and spinel facies. The most samples have medium- to coarse-grained protogranular textures. Tabular equigranular spinel lherzolite is also found occasionally. Many xenoliths contain hydrous minerals and metasomatic veins. Metasomatic veins in peridotites are composed of amphibole, phlogopite and pyroxenes in variable proportions (Litasov *et al.*, 2000c). Monomineral amphibole veinlets and interstitial amphibole and/or phlogopite in garnet and spinel lherzolites have been found. Clinopyroxene megacrysts and related pyroxenites can be divided into (Litasov *et al.*, 2000c): (1) Cr-rich megacrystic websterites and clinopyroxenites, and (2) Cr-poor megacrystic Gt-websterites, clinopyroxenites and Cpx-megacrysts, Al-Ti-Na-rich Cpx-megacrysts with ilmenite and phlogopite inclusions, and Ilmenite-Cpx-symplectites (graphic intergrowths). Samples from Miocene picrobasalts, selected for present study (Table 2), include garnet lherzolite (V-896), Cr-diopside spinel pyroxenite (P-7), spinel lherzolite with disseminated amphibole (V-706), and harzburgite with disseminated phlogopite (V-99).

Peridotite xenoliths from melaleucitites of Northern volcanoes of Udokan field (Ingamakit, Munduzhyak, Nizhni Lurbun, Neozhidany, note that last represents Pliocene basanites) are represented mainly by harzburgites. Lherzolite xenoliths are less abundant. Harzburgites often contain melt pockets, composed mostly of nepheline, leucite, sanidine or glass. Besides, fine chromite, rhonite, olivine, clinopyroxene, were found in these melt pockets (Sharygin *et al.*, 1998). Fe-rich clinopyroxenite series, composed mainly from dark-green elongated grains of clinopyroxene, is also detached (Litasov and Taniguchi, 2002).

Table 1. Representative compositions and age of host volcanic rocks from Baikal-Mongolian region.

	Vitim field				Oka field		Bartoy	Hamar-D.
Location	Bereya	Dzhilinda	Bulykhta	Kandidushka	Zabit	Yamata	Bartoy	Margasan
Source	[1]	[1]	[2]	[1]	[3]	[3]	[4]	[1]
Type	Picrobasalt	Basanite	Basanite	Basanite	Basanite	Basanite	Basanite	Basanite
Sample	C215	M-12/4	Bul	KN-23	S-2	S-4	B-1	HB-1
Age, Ma	16	1.8	1	0.9	3	3	1-3	8
SiO_2	41.8	46.3	45.1	44.1	47.7	47.8	44.0	46.6
TiO_2	2.11	2.16	3.41	2.38	2.23	2.41	2.44	2.15
Al_2O_3	9.5	13.2	14.5	13.2	15.6	15.4	14.7	17.0
FeO*	12.1	12.9	13.5	13.9	11.5	11.5	12.1	10.5
MnO	0.2	0.2	0.1	0.1	0.2	0.2	0.2	0.2
MgO	15.5	8.9	6.1	8.5	6.8	8.1	8.9	8.3
CaO	9.6	7.3	7.3	9.1	8.1	7.4	7.6	7.1
Na_2O	0.77	4.87	5.72	4.20	4.00	4.00	4.53	3.87
K_2O	1.46	2.69	3.71	2.68	2.29	2.65	2.70	2.04
P_2O_5	0.67	0.62	1.15	0.75	0.60	0.60	0.96	0.61
Total	93.7	99.1	100.6	99.0	99.0	100.1	98.1	98.4
Mg#	69.7	55.2	44.7	52.1	51.2	55.5	56.7	58.4

	Khentey	Udokan field					Taryat
Location	Burkal	Kuas	Ingamakit	Munduzhyak	N Lurbun	Neozhidany	S-Tsaram
Source	[5]	[6]	[7]	[8]	[7]	[7]	[9]
Type	Nephelinite	Basanite	Nephelinite	Nephelinite	Nephelinite	Basanite	Phono-basanite
Sample	Bu-1	U77-4	U-4	U-9	U-11	U-14	ST-4
Age, Ma	8	3	14	14	14	3	1.5
SiO_2	42.7	44.6	41.8	41.2	41.7	43.5	47.0
TiO_2	2.57	2.40	3.00	3.44	2.43	2.10	2.22
Al_2O_3	10.3	14.0	10.5	11.7	11.6	14.5	14.3
FeO*	11.8	11.2	12.2	12.0	11.3	14.3	10.1
MnO	0.2	0.2	0.2	0.2	0.2	0.2	
MgO	14.7	10.9	13.0	11.6	13.2	8.6	9.0
CaO	11.5	9.8	11.5	10.8	10.7	8.7	6.3
Na_2O	3.33	3.05	3.34	3.32	3.55	3.95	4.81
K_2O	1.96	1.21	2.60	3.18	2.30	2.40	4.23
P_2O_5	0.69	0.46	1.11	0.81	1.20	0.76	0.98
Total	99.7	97.7	99.1	98.1	98.1	99.0	99.0
Mg#	69.0	63.6	65.4	63.2	67.6	51.7	61.4

Sources: 1, Ashchepkov (1991); 2, Litasov and Taniguchi (2002); 3, Rasskazov et al. (1994); 4, Grachev (1998); 5, Rasskazov (1993); 6, Litasov et al. (1999b); 7, Stupak (1987); 8, Rasskazov et al. (1997); 9, Press et al. (1986). FeO*, total Fe as FeO (here and in following tables). Mg#=100xMg/(Mg+Fe).

Table 2. Sample numbers, petrography, and localities of xenoliths comprising this study.

Sample	Rock type	Locality	Texture	Modal composition							T, BK-1	T, BK-2	N-LT
				Ol	Op	Cp	Sp	Gt	Am	Ph			
	Vitim field												
D-51	Gt-Sp lherzolite	Dzhilinda	P/M	65	15	17	1.7	1			1082	922	
D-11	Sp harzburgite	Dzhilinda	P/C	78	18	3	1				772	905	
D-82	Sp lherzolite	Dzhilinda	P/C	62	18	17	2.1				1079	1023	181
D-3F	Sp lherzolite	Dzhilinda	P/C	64	19	14	2				1140	986	
D-19	Sp lherzolite	Dzhilinda	T/F	49	32	16	3				830	922	200
D-2	Sp lherzolite	Dzhilinda	M/F	46	34	14	5				886	787	
DY-8A	Sp lherzolite	Dzhilinda	M/F	46	33	17	3				859	802	204
BL-32	Gt-Sp lherzolite	Bulykhta	P/M	58	12	12	0.2	17			1115	1010	245
Ka-2	Sp lherzolite	Kandidushka	P/M	61	22	13	2				1133	996	296
Ka-101	Sp lherzolite	Kandidushka	P/C	71	19	8	1				1119	976	293
V-896	Gt-Sp lherzolite	Bereya Quarry	P/C	49	29	11	1	10			1174	1034	
P-7	Sp pyroxenite	Bereya Quarry	CE/C	8	31	54	3				1264	983	
V-706	Am-Sp lherzolite	Bereya Quarry	P/C	53	23	8	2		2.5		1134	1003	068
V-99	Ph Harzburgite	Bereya Quarry	Ph/M	71	20					7		787	
	Udokan field												
In-40	Sp harzburgite	Ingamakit	P/F	77	17	3	2				940	828	533
106-16	Sp harzburgite	Ingamakit	Ph/M	81	12	1	2				869	834	
106-22	Sp harzburgite	Ingamakit	P/M	76	17	2	3				833	1091	531
106-26	Sp harzburgite	Ingamakit	P/M	85	13		1					934	
M-7	Sp lherzolite	Munduzhyak	P/M	66	13	9	1				812	923	534
N2-1	Sp harzburgite	Neozhidany	P/M	78	15	6	0.2				961	926	542
U19-12	Sp lherzolite*	N Lurbun	P/M								957	847	543
74-11	Sp harzburgite	Kuas	P/C	74	21	3	2				1049	975	493
74-24	Sp harzburgite	Kuas	P/M	70	22	6					1058	948	491
	Oka field (Sayan)												
K-15	Sp lherzolite	Zabit	P/C	70	21	8	1.2				1021	939	330
K-60	Websterite	Zabit	P/C		91	8					1126	1000	337
	Hamar-Daban												
X-13	Sp lherzolite	Margasan	T/F	59	26	12	2				982	943	
X-24	Sp lherzolite	Margasan	P/C	71	6	20	1				1082	956	375
X-06	Ol-websterite	Margasan	CE/C	8	33	58					1004	955	396
	Bartoy field												
B-002	Am-Sp wehrlite	Bartoy	P/M	87	2	7	1.5		4				411
B-012	Am-Sp lherzolite	Bartoy	P/M	65	22	8	0.5		1		1042	950	407
B-401	Ph-Sp lherzolite	Bartoy	P/M	60	20	15	1.6			3.4	1103	1145	416
	Khentey												
Bu-15	Gt-Sp lherzolite	Burkal	P/M	57	19	18	1	4			1150	1053	461
Bu-11	Sp lherzolite	Burkal	P/M	64	25	8	1				1113	1009	479
Bu-30	Sp lherzolite	Burkal	P/M	62	23	13	1				1114	1050	478
	Taryat												
SHT-36	Sp lherzolite	Shav.-Tsaram	P/F	60	22	17	1				948	851	562
SHT-5	Sp lherzolite	Shav.-Tsaram	P/M	71	16	11	1				942	836	565

Textures: P, protogranular; Ph, porphyroclastic; T, tabular-equigranular; M, mosaic-equigranular; CE, coarse-equant. Grain size: C, coarse (Ol, Op, Cp typically >5 mm); M, medium (1-5 mm); F, fine (<1 mm). Minerals: Ol, olivine; Op, orthopyroxene; Cp, clinopyroxene; Sp, spinel; Gt, garnet; Am, amphibole; Ph, phlogopite. T, temperatures (°C) after Brey and Kohler (1990) two-pyroxene (BK-1) and Ca-orthopyroxene (BK-2) thermometers. N-LT, sample numbers for primary minerals in Litasov and Taniguchi (2002), appendix 3. The other xenoliths minerals are presented in table 3. *, Modes were not determined.

Table 3. Representative analyses of primary mineral phases in selected xenoliths.

Sample	D-51			D-11				D-3F				D-2			
Mineral	ol	op	cp	ol	op	cp	sp	ol	op	cp	sp	ol	op	cp	sp
SiO_2	40.87	54.76	52.2	40.78	56.12	52.87		40.39	54.88	52.32		41.3	55.43	51.47	
TiO_2	0.02	0.09	0.34		0.05	0.13	0.10		0.08	0.26	0.13		0.19	1.95	0.22
Al_2O_3		4.32	6.06		2.94	2.65	43.39		4.58	5.91	51.22		3.41	7.13	53.05
Cr_2O_3	0.02	0.42	0.83		0.44	0.74	25.21	0.01	0.53	1.01	16.58		0.37	1.12	15.32
FeO	9.32	5.97	2.88	8.31	4.89	1.94	13.24	9.25	5.95	3	12.42	8.36	5.5	1.96	10.46
MnO	0.11	0.15	0.1	0.09	0.12	0.07	0.07	0.11	0.15	0.11	0.11	0.08	0.15	0.07	0.1
MgO	49.84	33.52	15.37	50.67	34.83	16.85	17.69	49.94	32.57	16.05	19.45	50.19	34	13.88	18.92
CaO	0.09	0.66	18.92	0.03	0.59	22.94		0.08	0.84	18.62	0	0.04	0.31	20.56	0.65
Na_2O	0.01	0.13	1.86		0.02	0.79			0.18	1.6			0.05	1.92	
NiO	0.3			0.45			0.35	0.34			0.36	0.58			0.61
Total	100.6	100	98.56	100.3	100	98.98	100.1	100.1	99.76	98.88	100.2	100.6	99.41	100.1	99.33
Mg#	90.5	90.9	90.5	91.6	92.7	93.9	70.4	90.6	90.7	90.5	73.6	91.5	91.7	92.7	76.3

Sample	V-896				P-7				V-99		
Mineral	ol	op	cp	gt	ol	op	cp	sp	ol	op	ph*
SiO_2	40.93	54.93	52.23	42.74	40.85	55.1	52.28	0.03	40.4	54.94	40.4
TiO_2	0.01	0.17	0.55	0.22	0.02	0.14	0.41	0.57	0.07	0.11	2.73
Al_2O_3	0.02	4.55	6.23	23.28	0.01	3.91	5.68	53.55		3.1	14.13
Cr_2O_3		0.59	1.29	1.25	0.04	0.57	1.35	12.87	0.01	0.34	0.44
FeO	9.63	5.97	3.17	7.39	9.64	6.01	3.12	11.94	12.1	8.53	3.59
MnO	0.12	0.11	0.08	0.28	0.14	0.16	0.12	0.09	0.14	0.14	
MgO	49.28	33.01	16.43	20.53	48.92	32.97	15.85	20.24	47.13	31.52	22.89
CaO	0.08	0.94	17.89	5.03		0.83	18.56		0.11	0.31	0.04
Na_2O		0.08	1.91		0.02	0.17	1.9		0.05	0.06	1.22
K_2O		0.01	0.01		0.01		0.01				9.32
NiO	0.39	0.02	0.01	0.07				0.17	0.13		
Total	100.4	100.4	99.8	100.8	99.64	99.86	99.28	99.46	100.2	99.05	94.76
Mg#	90.1	90.8	90.2	83.2	90	90.7	91.4	75.1	87.4	86.8	91.9

Sample	106-16				106-26			X-13			
Mineral	ol	op	cp	sp	ol	op	sp	ol	op	cp	sp
SiO_2	40.93	56.44	52.99		40.89	56.55	0.12	40.98	55.61	53.00	0.18
TiO_2		0.08	0.18	0.14	0.02	0.03	0.41	0.03	0.08	0.54	0.19
Al_2O_3		2.59	2.98	40.05		2.37	6.72		4.44	7.41	58.49
Cr_2O_3		0.36	0.67	26.74		0.34	55.00		0.31	0.80	9.25
FeO	8.62	5.66	2.24	15.61	8.56	5.03	25.89	9.94	6.26	2.91	10.47
MnO		0.14	0.07	0.11	0.12	0.10	0.14	0.17	0.10	0.09	0.11
MgO	49.82	34.42	16.66	16.95	49.78	34.52	10.12	49.10	32.28	14.56	21.22
CaO	0.01	0.41	22.50		0.03	0.67	0.01	0.09	0.73	18.87	
Na_2O		0.02	0.70			0.11			0.17	2.19	
NiO	0.35			0.29	0.33		0.13	0.40	0.16	0.02	0.43
Total	99.73	100.1	98.99	99.89	99.73	99.73	98.54	100.7	100.1	100.4	100.3
Mg#	91.1	91.6	93.0	65.9	91.2	92.4	41.1	89.8	90.2	89.9	78.3

See table 2 for explanations. *, Phlogopite contains also F=3.44 wt.%

Cr-diopside group xenoliths from Pliocene basanites of Central Udokan field (Kuas Lake) may be divided into spinel lherzolites, spinel harzburgites and dunites, and spinel websterites and related pyroxene-rich lherzolites. Nodules with partly recrystallized clinopyroxene and spinel were found within the harzburgite group. One spinel-free harzburgite (sample U74-24) contain pink post-garnet kelyphite aggregates and has strongly spongy-rimmed clinopyroxene with abundant fluid and melt inclusions.

Mantle xenoliths of Oka volcanic field (Sayan) include anhydrous spinel and garnet lherzolites. Various Cr-diopside pyroxenites with high amount of orthopyroxene (Opx=70–90 mod.%) are also abundant. We studied glasses in typical spinel lherzolite and websterite (Table 2). Same xenolith suites are characteristic for Hamar-Daban localities. They contain minor garnet-bearing varieties but include depleted harzburgite and foliated peridotites with abundant interstitial feldspar-bearing veins and melt pockets (Ionov *et al.*, 1995).

Spinel lherzolites, including amphibole-bearing varieties, are most abundant in the Bartoy location (Litasov *et al.*, 2000d). Clear similarities were observed for xenolith types, mineral compositions, and xenoliths' metasomatic modification between Bartoy Pliocene basanites and Vitim Miocene picrobasalts. Several types of metasomatic modification of Bartoy xenoliths were detected using trace element characteristics of clinopyroxene and amphibole: 1) disseminated amphibole in modally depleted lherzolites; 2) disseminated amphibole and/or phlogopite in lherzolites and Cr-diopside pyroxenites; 3) amphibole-phlogopite and amphibole-phlogopite-pyroxene vein-rocks often crosscutting the lherzolites. In the present study we considered glass-bearing pockets from amphibole and phlogopite-bearing xenoliths (Table 2).

Mantle xenoliths in the melaleucitites of Burkal River include dry and hot (T=1100–1150°C) garnet and spinel lherzolites. Although host rock is the same with Northern Udokan volcanoes and melaleucitite is known as very reactive melt, mantle xenoliths contain less products of reactions and are almost free from any melt pockets and other xenolith modifications.

Xenoliths suite of the Shavaryn-Tsaram volcano in Central Mongolia is generally resembles that of Vitim (Bereya Quarry) and Bartoy volcanic fields, however, hydrous metasomatic modification is less widespread (Litasov and Taniguchi, 2002). Metasomatized anhydrous spinel lherzolites often contain spongy rims around clinopyroxene and spinel and interstitial glasses and melt pockets along grain boundaries (Ionov *et al.*, 1994).

5. Mineralogy of host volcanic rocks

Most glasses and melt pockets in mantle xenoliths are formed due to reaction with host magma in the depth or during transport to the surface and subsurface crystallization. It is important to study mineralogy of host rock to compare compositions of their minerals and those observed in xenolith's microlites. Mineralogy of the alkaline basalts was studied in details for Vitim and Udokan volcanic field (e.g. Sharygin *et al.*, 1998; Litasov *et al.*, 2002) and partially for Hamar-Daban and Burkal localities (section 7).

In the Vitim volcanic field basanites of the Dzhilinda and Bulykhta contain clinopyroxene and olivine phenocrysts ranging in 0.4–1.5 cm. The groundmass consists of clinopyroxene, olivine, Ti-magnetite, plagioclase, apatite, and albite. It also includes small patches (less than 1–2 mm in diameter) of cryptocrystalline K-bearing mixture of

crystals and glass. Glasses of unheated primary melt inclusions in olivine phenocrysts from Dzhilinda basanite contain 58–63 wt.% SiO_2, 9–11 wt.% of alkalies (Alk#=Na_2O+K_2O), and has Mg#=37–46 (No D–22 in Table 4). Homogenization temperatures of these melt inclusions are ranged from 1100 to 1150℃ and associated CO_2 fluid inclusions have density of 0.76–0.86 g/cm^3. Scoria basanite of the Kandidushka volcano contain olivine, clinopyroxene, and rare plagioclase submerged in the matrix glass. Matrix glass contain 50-54 wt.% SiO_2, 7–10 wt.% of Na_2O+K_2O, and has Mg#=18–35 (Table 4).

Picrobasalt from the Bereya Quarry are overfilled of different phenocrysts including many from disintegrated mantle and crustal xenoliths. Some of the phenocrysts with sufficiently low Mg number and lack of zoned reaction rims can be attributed to picrobasalt crystallization. They include Fe-rich olivine, Al-rich clinopyroxene, plagioclase, chromite, Ti-magnetite (Table 6). Surprisingly, picrobasalt matrix glass is Si-rich, containing 55–61 wt.% SiO_2, 2.1–2.5 wt.% CaO, 4.0–4.5 wt.% K_2O, and has Mg#=47–55 (Litasov *et al.*, 2002).

Melaleucitites/melanephelinites of Northern Udokan contain clinopyroxene (Mg#=85–90) and olivine (Mg#=75–85) phenocrysts. Groundmass consists of olivine (Mg#=70–75), Ti-augite (Mg#=80-85), titanomagnetite (TiO_2=12–25 wt.%), F-apatite, Ba-Ti-biotite, nepheline, leucite, and rarely ilmenite, K-feldspar and glass. Some varieties (pegmatoid nephelinite) contain perovskite and aegirine. Calcite is typical postmagmatic phase in all melanephelinites.

6. Petrography and chemistry of fluid and melt inclusions

6.1. Type I (early) inclusions

Unlikely to interstitial glasses fluid and melt inclusions provide direct information about deep mantle processes because complete isolation of melt/fluid by host mineral after trapping. We studied fluid and melt inclusions in minerals from Vitim, Udokan and Hamar-Daban xenoliths. We studied also only fluid inclusions in minerals from Bartoy and Burkal xenoliths.

Associated fluid and melt inclusions can be divided into early (Type I) and late (Type II). Type I includes rare primary and pseudosecondary melt and fluid inclusions (Fig.1). Primary inclusions are relatively large (5–15 mm) and occur isolated from any other inclusions or healed fractures. Pseudosecondary inclusions have same size and formed along healed fractures. These fractures have early origin and only several inclusions are usually included into one group. Melt and fluid inclusions of type I often have negative crystal shape and contain glass, daughter minerals and gas bubble. Sometimes they contain no visible phases except solid glass. The fluid inclusions usually contain glass and gas bubble. Clinopyroxene, Cr-spinel, and sulfide occur as daughter minerals in inclusions. Primary and pseudosecondary inclusions of type I have homogenization temperatures (T_{hom}) of 1200-1280℃. Some primary inclusions in Kandidushka (Vitim) and Bartoy xenoliths have lower T_{hom} of 1150-1200℃. According to previous data on gas chromatography (Simonov *et al.*, 1992) and melting temperature of fluid inclusions (−56–57℃), we can conclude that the fluid inclusions consist of pure CO_2.

In the Vitim field maximum density of CO_2 in the fluid inclusions is near 1.00 g/cm^3 for Dzhilinda xenoliths, and up to 1.18 g/cm^3 for Kandidushka and Bereya Quarry xenoliths. Many fluid inclusions of type I have decrepitating aureoles; some of them have

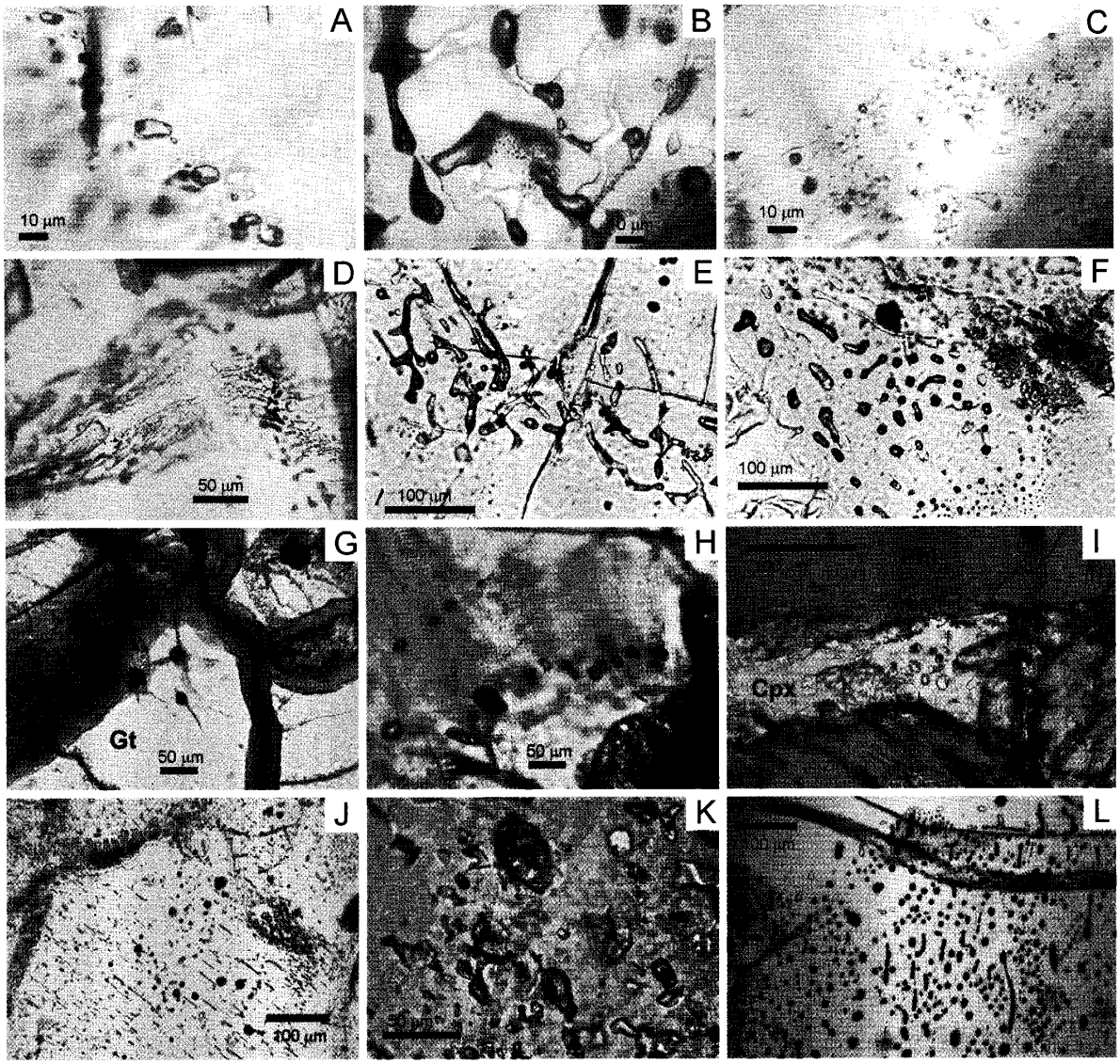

Figure 1. Photomicrographs of melt and fluid inclusions in Baikal xenoliths. A-F, Dzhilinda, Vitim field: A, series of pseudo-secondary fluid inclusions in olivine, sample D-51. B, complex vermicular net of fluid and melt inclusions in orthopyroxene, sample D-19. C, pseudo-secondary fluid inclusions in orthopyroxene, sample D-2. D, zones of secondary fluid and melt inclusions in olivine, sample D-2. E, fluid inclusions in clinopyroxene, composed of glass + gas bubble, sample DY-8A. F, negative crystal shape inclusions in olivine, sample DY-8A. G, primary melt inclusions in garnet with radial decrepitating cracks, Bulykhta (Vitim field), sample BL-32. H, primary or pseudo-secondary melt and fluid inclusions in clinopyroxene from garnet lherzolite, Bereya Quarry (Vitim field), sample V-896. I, series of primary or pseudo-secondary melt and fluid inclusions in clinopyroxene from phlogopite-bearing vein, Bereya Quarry (Vitim field), sample V-857. J, abundant fluid and melt inclusions in olivine, Hamar-Daban, sample X-06. K-L, Ingamakit (Udokan field): K, fluid and melt inclusions in clinopyroxene, sample 106-16. L, series of fluid inclusions in primary olivine, sample 106-26.

density up to 1.14g/cm^3 suggesting very high initial pressure of trapping. The melt inclusions sometimes explode during heating experiments and prevent the achivement of homogenization temperatures. This fact is also support very high-pressure and high-temperature origin of the inclusions. Orthopyroxene and rarely olivine, clinopyroxene and garnet are the host minerals for primary and pseudosecondary melt and fluid inclusions (Fig.1). It should be noted that clinopyroxene megacrysts and high-temperature Cr-rich megacrystic websterites from Bereya picrobasalts contain large rounded vugs up to 5 mm in size, probably representing former fluid inclusions, some of them are partially filled by sulfide (monosulfide solid solution and pentlandite).

The density of selected pseudosecondary CO_2 inclusions in minerals of Udokan xenoliths is typically 1.00–1.05 g/cm^3 (T_{hom}=1200–1220℃). The density range for Burkal xenoliths is 1.07–1.10 g/cm^3. Bartoy xenoliths contain minerals with very dense CO_2 (up to 1.16g/cm^3). Most melt inclusions from Burkal xenoliths explode near 1250℃ indicating their high TP-origin (see section 9.1).

The composition of glasses from unheated and heated melt inclusions associated with fluid inclusions of type I varies widely. Fig.2 shows compositions of glasses from heated and residual melt inclusions along with interstitial glasses for Vitim xenoliths. The glasses from heated inclusions of type I contain low SiO_2, Na_2O, K_2O, and high FeO, MgO, and CaO relative to glasses from unheated inclusions. Glasses from heated inclusions in the Dzhilinda peridotites of series 1 and 2 have Mg#=66–88 and contain SiO_2=52–59 wt.%, TiO_2=0.4–1.4 wt.%, K_2O<2 wt.%. Glasses from heated inclusions in Ti-rich peridotites of series 3 contain up to 5.1 wt.% of TiO_2. Composition of glasses from unheated melt inclusions in Dzhilinda xenoliths is very similar with those of interstitial glasses (Fig.2).

The glasses from melt inclusions from garnet peridotite V-896 (Bereya Quarry) are thought to represent deepest trapped melt in the Vitim samples (Table 5). The glasses from heated inclusions have Mg#=63–70 and contain SiO_2=49–51 wt.%, TiO_2=1.1–1.5 wt.%, K_2O=1.9–2.5 wt.%. They also have high FeO, MgO, and CaO relative to glasses from unheated inclusions of the same sample (Fig.2).

Some melt inclusions from clinopyroxene in amphibole-bearing spinel lherzolite from Bartoy (sample B–012) have primitive compositions similar with those observed in V-896. However, they contain more K_2O and Na_2O (Fig.3). This can reflect amphibole melting during formation of inclusions.

6.2. Type II (late) inclusions

Type II includes numerous secondary and rarely pseudo-secondary melt and fluid inclusions. These inclusions form complicated trails, zones along healed fractures, intricate vermicular network in xenolith minerals, and have size up to 200 μm (Fig.1). Thickness of the inclusions, however, is not exceed 10–30 mm. Vermicular channels, especially within spongy rims of clinopyroxene from Dzhilinda lherzolites are often filled by plagioclase±sanidine and associate with fluid inclusions, containing liquid CO_2 and gas bubbles. Secondary melt inclusions of type II have homogenization temperatures of 1000–1190℃. Density of CO_2-inclusions varies from 0.55 to 0.82 g/cm^3.

Only several glasses from pseudo-secondary melt inclusions of type II were analyzed. In Dzhilinda samples (Vitim field) they have intermediate composition between residual glasses in melt inclusions of type I, interstitial glasses, and the host

basanites. For example, pseudosecondary melt inclusions in olivine from D-51 are clearly correspond to the type II, because composition of glasses from heated inclusions is very similar with host basanite (Table 4 and Fig.2).

Minerals of Dzhilinda harzburgite D-11 contain pseudo-secondary melt inclusions of type II with Si-rich glass (SiO_2=65-72 wt.%). The glasses have Mg#=50-65, and low TiO_2=0.1-0.3 wt.%, K_2O content decrease with increasing SiO_2 (Fig.2). The composition of similar glasses in melt inclusions from Udokan harzburgites (Ingamakit, Kuas) is consistent with composition of interstitial glasses from same xenoliths (Fig.3). They contain SiO_2=65-74 wt.% and typically rich in K_2O (up to 10 wt.%).

7. Petrography and chemistry of glasses in veinlets and melt pockets

Composition of glasses in xenoliths and host basalts are shown in Table 4-5 and Fig.2-3. Variety of interstitial glasses can be divided into interstitial veinlets and melt pockets. We do not consider here thick interstitial veins and melt leakages, which have clear connections with host basalts. There are considerable evidences that most studied glasses are in equilibrium with peridotite minerals, whereas the basaltic glasses are not. Studied glasses have usually equilibrium sharp contacts with peridotite minerals (e.g. Fig.4A, F-H, Fig.5A-E) in contrast to reactionary contacts between xenoliths and infiltrating basaltic glass (e.g. Fig.4C,E). Furthermore, the compositions of microlites in highly silicic glass are similar to those of the main phases in the host xenolith (Mg-rich olivine, Cr-spinel, Cr-diopside (Table 6-9), whereas those in basaltic glass are not (Ti-Fe-rich augite, Fe-rich olivine, Ti-magnetite or chromite in picrobasalt). Composition of xenolith and basaltic glasses are also different, for example, boundary zones in D-82, D-3F, and Ka-2 (Vitim field), contain basalt-related Ti-magnetite and glasses with 49-57 wt.% SiO_2 whereas inner zone contain Cr-spinel among microlites and glasses with 58-72 wt.% SiO_2.

7.1. Vitim field

Interstitial patches (melt pockets) in the Dzhilinda and Kandidushka xenoliths occur around spongy-rimmed clinopyroxene (Fig.4A) and spinel grains, and consist of secondary clinopyroxene+plagioclase+sanidine. Melt pockets with glass are more rarely in Dzhilinda and frequently observed in Kandidushka xenoliths. Glasses in melt pockets in lherzolite xenoliths are usually associated with euhedral clinopyroxene, olivine, and Cr-spinel microlites. Thin interstitial veinlets rarely contain microlites, however, in Dzhilinda peridotites many veinlets are represented by plagioclase ± sanidine, which supposed to be former glass or melt.

Compositions of glasses in melt pockets and veinlets of the Dzhilinda and Kandidushka xenoliths are generally similar. However, veinlet glasses related to orthopyroxene-olivine grain boundaries in depleted lherzolite and harzburgite nodules contain high SiO_2 (61-71 wt.%) relative to melt pocket glasses (55-61 wt.% SiO_2) (Fig.2). It should be noted, that interstitial glasses and glasses from melt inclusions in minerals of fertile lherzolites (D-51, D-19, D-2) are similar in composition with glasses from primary melt inclusions in olivine phenocrysts from Dzhilinda basanite (Fig.2).

Glasses of interstitial veinlets and melt pockets from garnet and spinel-bearing xenoliths from Bereya Quarry contain SiO_2=55-65 wt.%, and have high FeO (2.1-4.2 wt.%), MgO (0.8-2.8 wt.%), CaO (5.1-6.9 wt.%) (Fig. 2).

Glasses in spinel lherzolite V-706 occur in melt pockets around disseminated amphibole grains (Fig.4F). Some melt pockets in xenoliths contain no amphibole or include relic amphibole appearing like shadow in the central part of the melt pocket. The glass in V-706 is certainly formed by amphibole melting and contains euhedral clinopyroxene, olivine, and Cr-spinel microlites. The glass is characterized by high SiO_2 (53–58 wt.%) and TiO_2 (1.9–2.5 wt.%) has Mg#=50–58 and Alk# (total alkalis) =2.8–7 wt.% (Fig.2).

Glasses in harzburgite V-99 were observed in melt pockets around phlogopite grains, and can be related to phlogopite melting (Fig.4G). This glass contains ilmenite needles in the boundary zones. Phlogopite in the sample is supposed to have metasomatic origin unrelated to primary assemblage. It has Mg#=92, while olivine and orthopyroxene have Mg#=86–87. These features, i.e. melting of phlogopite and occurrence in depleted xenoliths, produce glasses with specific composition. From the one side they have high SiO_2 (63–68 wt.%) and Na_2O (4–6 wt.%) and low FeO (0.25–1.0 wt.%) and MgO (0.2–0.5 wt.%), which is characteristic for Si-rich glasses in harzburgites, but from the other side they have high TiO_2 (0.7-1.6 wt.%) and K_2O (6–11 wt.%), which is typical for glasses formed by phlogopite melting (Fig.2).

Glasses of interstitial veinlets and melt pockets from garnet and spinel-bearing xenoliths from Bereya Quarry contain SiO_2=55–65 wt.%, and have high FeO (2.1–4.2 wt.%), MgO (0.8–2.8 wt.%), CaO (5.1–6.9 wt.%) and form different SiO_2-K_2O-trend relative to Si-rich matrix glasses from picrobasalt (Fig.2).

7.2. Udokan field

Melt pockets are very abundant in harzburgite xenoliths from melanephelinite volcanoes of Udokan volcanic field (Fig.5) (Sharygin *et al.*, 1998). However, they are typically composed of recrystallized mineral assemblies (see section 8.2) and contain no glasses. Even majority of melt inclusions in the minerals are presented by recrystallized mineral phases like leucite, sanidine and nepheline. Rare interstitial glasses from harzburgites of Ingamakit and Munduzhyak volcanoes are different those from spinel lherzolite of Nizhni Lurbun). They have similarly high SiO_2 (69–74 wt.%), but contain significantly higher K_2O (6–10 wt.% and 3–4 wt.% respectively). Interstitial glasses from Kuas harzburgite (74–11) are generally resemble these compositions (64–68 wt.% of SiO_2 and 3.5–5.0 wt.% of K_2O, Table 5, Fig.3).

7.3. South Baikal and Mongolia

Ionov *et al.* (1994) described metasomatic glasses in mantle xenoliths from Shavaryn-Tsaram volcano and Dariganga volcanic field (Fig.3). Glasses were detected in melt pockets around spongy-rimmed clinopyroxene of spinel lherzolites. They contain 51–65 wt.% SiO_2, 1.7–7.0 wt.% CaO, 7–11 wt.% Na_2O, 0.8–4.0 wt.% K_2O. Microlite of clinopyroxene, olivine, and Cr-spinel are usually associated with glasses. We detected also glass-bearing veinlets in some Hamar-Daban xenoliths. The glasses are K-rich (Fig.3, Table 6) and contain 66–69 wt.% SiO_2, 3.3–4.0 wt.% Na_2O and 5.4–6.6 wt.% K_2O.

8. Petrography and chemistry of microlites in veinlets and melt pockets

Melt pockets and veins in lherzolite xenoliths are usually associated with euhedral clinopyroxene, olivine, and Cr-spinel microlites. They also contain glass or one or more

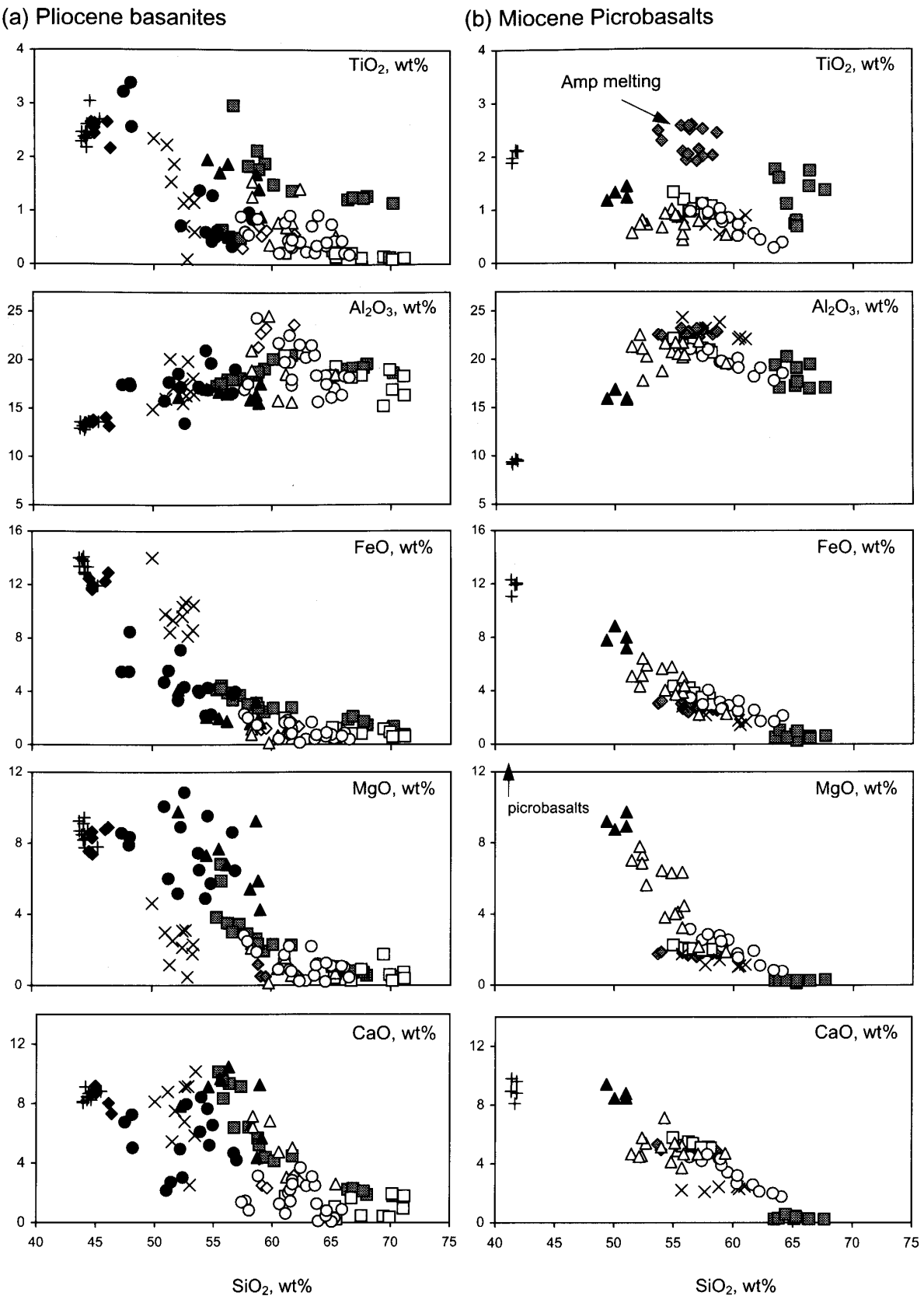
(a) Pliocene basanites
(b) Miocene Picrobasalts
TiO2, wt%
Amp melting
Al2O3, wt%
FeO, wt%
MgO, wt%
picrobasalts
CaO, wt%
SiO2, wt%
SiO2, wt%

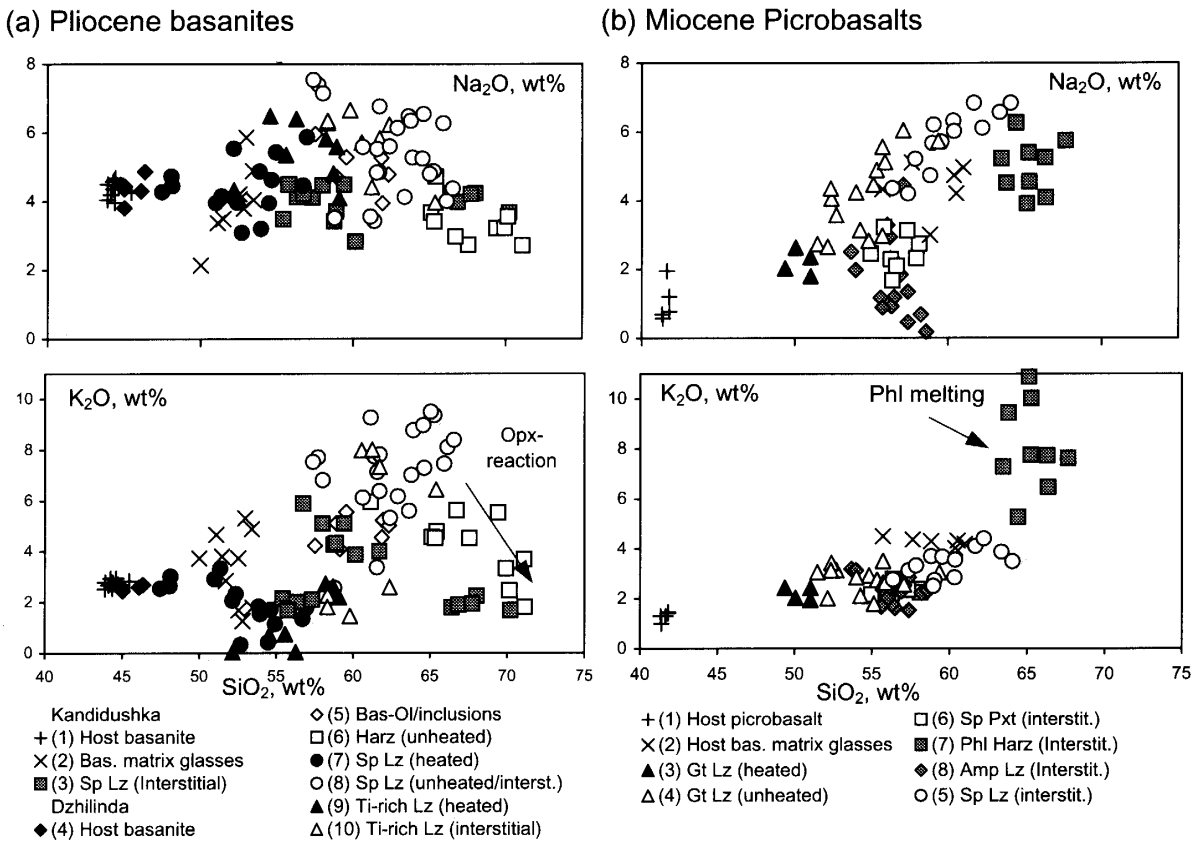

Figure 2. Composition variations vs SiO_2 content in glasses in mantle xenolith from Vitim volcanic field. (A) Pliocene basanites: Kandidushka volcano: (1) composition of host basanite; (2) matrix glass in basanite; (3) interstitial glass in spinel lherzolite. Dzhilinda: (4) composition of host basanite; (5) residual (unheated) melt inclusions in olivine phenocryst of basanite; (6) residual melt inclusions in minerals from harzburgite D-11; (7) heated melt inclusions in spinel lherzolites of series 1 and 2; (8) unheated melt inclusions and interstitial glasses in spinel lherzolites of series 1 and 2; (9) heated melt inclusions in Ti-rich spinel lherzolite of series 3; (10) interstitial glasses in Ti-rich spinel lherzolite of series 3. (B) Miocene picrobasalts, Bereya Quarry: (1) host picrobasalt; (2) matrix glass in picrobasalt, (3) heated melt inclusions in garnet lherzolite V-869; (4) unheated melt inclusions in garnet lherzolite; (5) interstitial glass in spinel lherzolite; (6) interstitial glass in spinel pyroxenite P-7; (7) interstitial glass in amphibole-bearing lherzolite V-706; (8) interstitial glass in phlogopite-bearing harzburgite V-99.

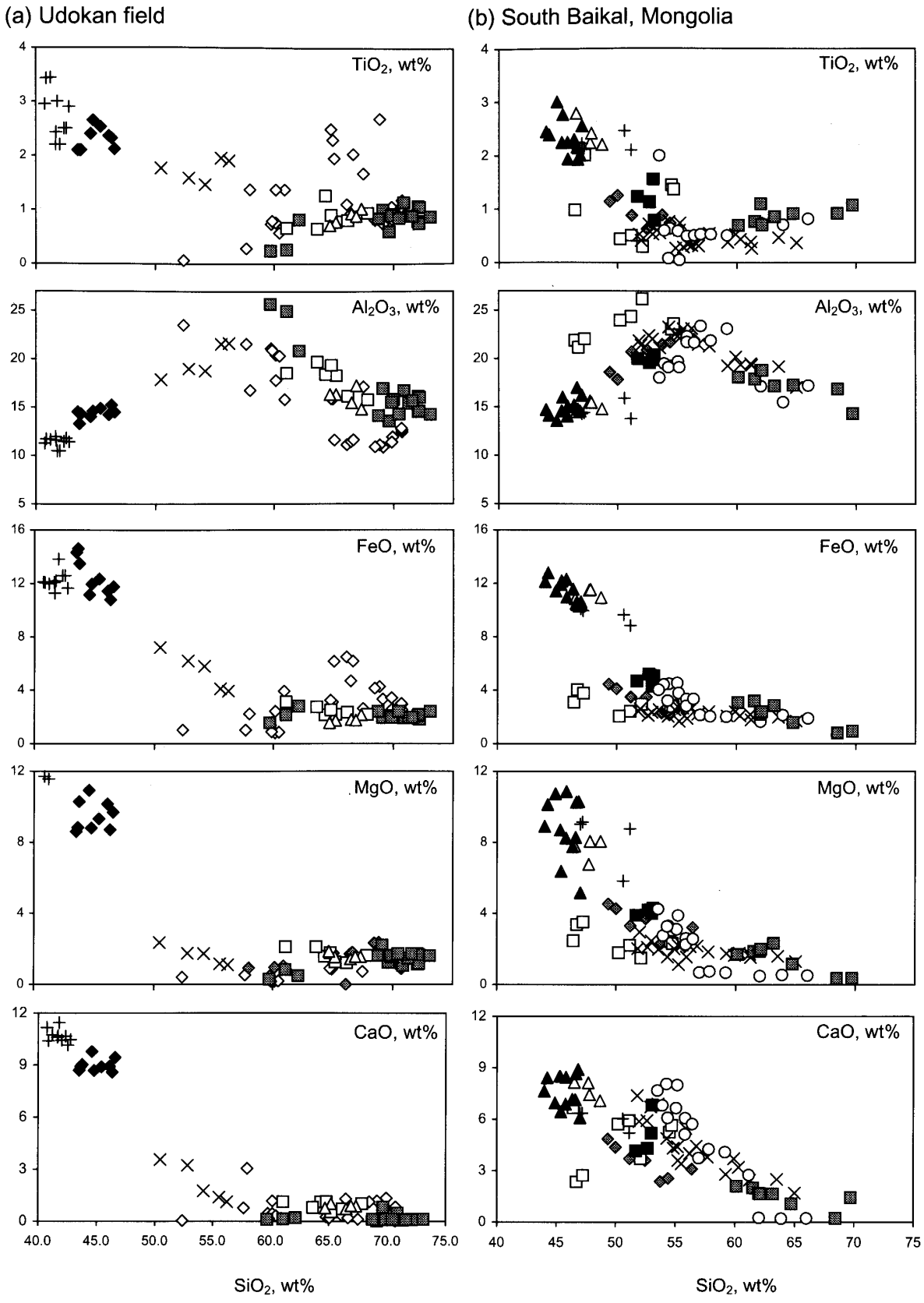
(a) Udokan field
(b) South Baikal, Mongolia
TiO2, wt%
Al2O3, wt%
FeO, wt%
MgO, wt%
CaO, wt%
SiO2, wt%
SiO2, wt%

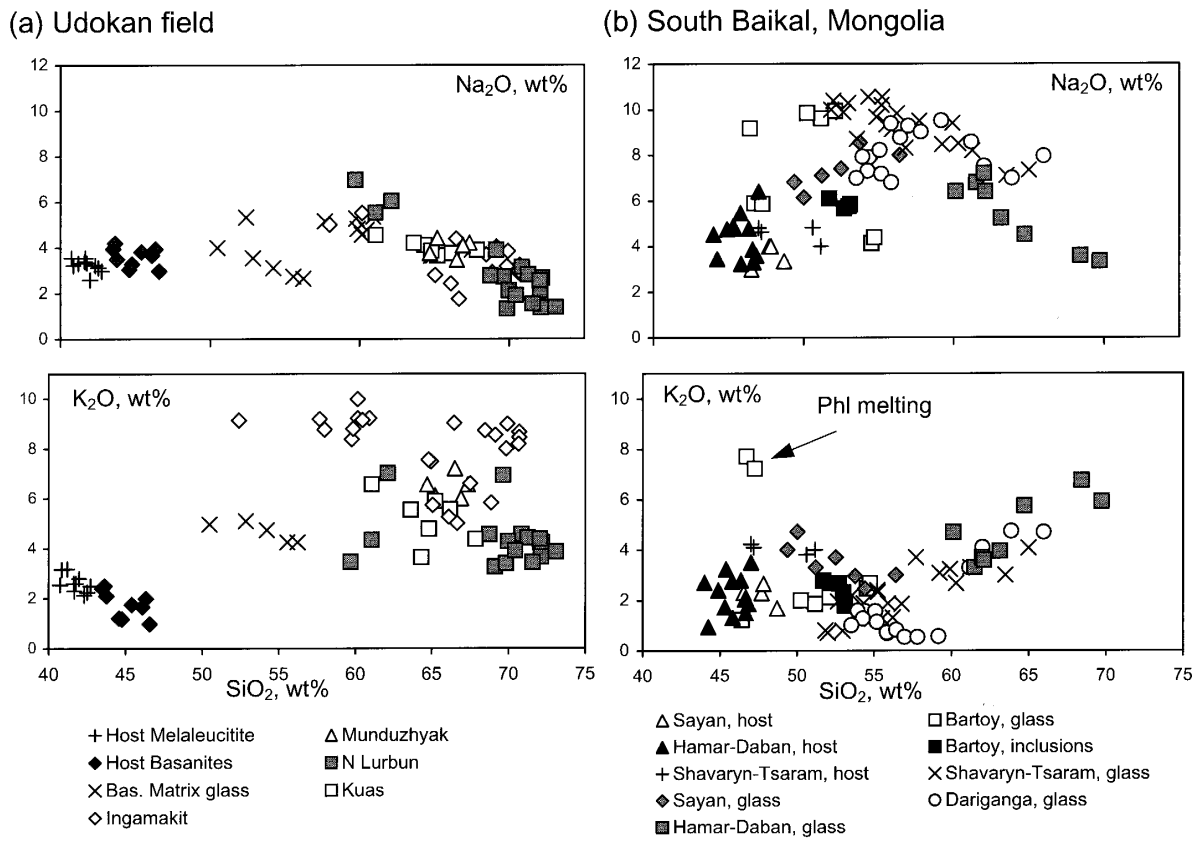

Figure 3. Composition variations vs SiO_2 content in glasses in mantle xenolith from Udokan, South Baikal and Mongolia. Bas. matrix glass, groundmass glass in melaleucitites. Note that Ingamakit includes interstitial glasses and melt inclusions in olivine and N Lurbun includes melt inclusions in primary and secondary olivine and interstitial glasses.

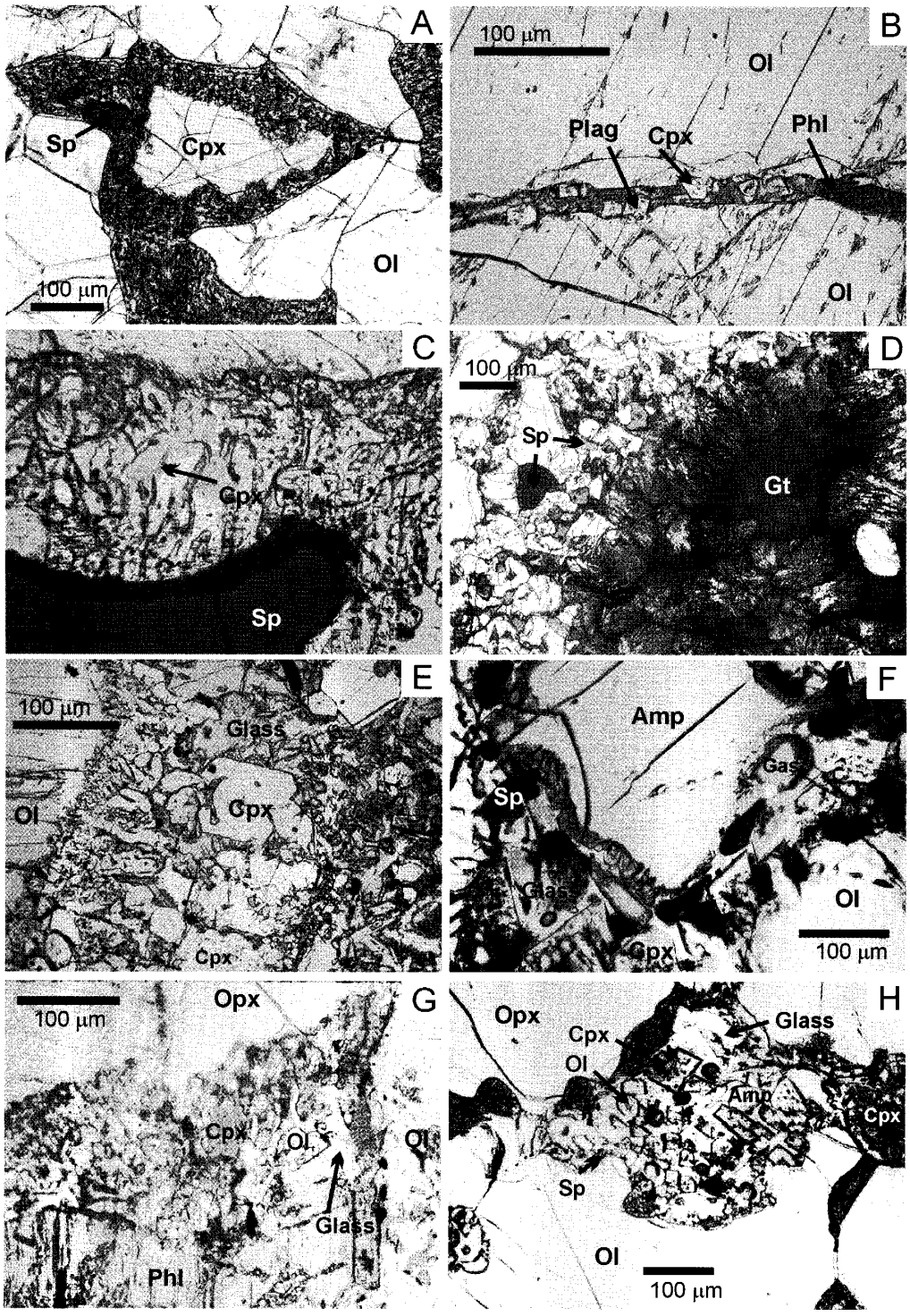

Figure 4. Photomicrographs of Vitim and Bartoy xenoliths. Vitim volcanic field: A-E, Dzhlilinda; F-G, Bereya Quarry. A, spongy rim around clinopyroxene bearing in fluid and melt inclusions, sample D-82. B, interstitial veinlet between olivine grains, Sample D-3F; C, clinopyroxene microlites and glass near spinel grain, sample D-3F. D, spinel lherzolite with porphyroclastic microstructure and two different spinels, primary brown spinel and secondary yellow-brown spinel formed in kelyphitic aggregates after garnet, sample 628-16. E, formation of clinopyroxene microlites and glass near the xenoltih/basalt boundary, Sample D-3F. F, glass-bearing melt pockets around amphibole, sample V-706. G, Glass-bearing melt pocket near phlogopite grain in Fe-rich phlogopite harzburgite, sample V-99. H, Bartoy filed, melt pocket in amphibole-spinel lherzolite bearing in clinopyroxene and olivine microlites, sample B-012. Abbreviations: Cpx, clinopyroxene; Opx, orthopyroxene; Gt, garnet; Sp, spinel; Amp, amphibole; Plag, plagioclase; Phl, phlogopite; Gas, gas bubble.

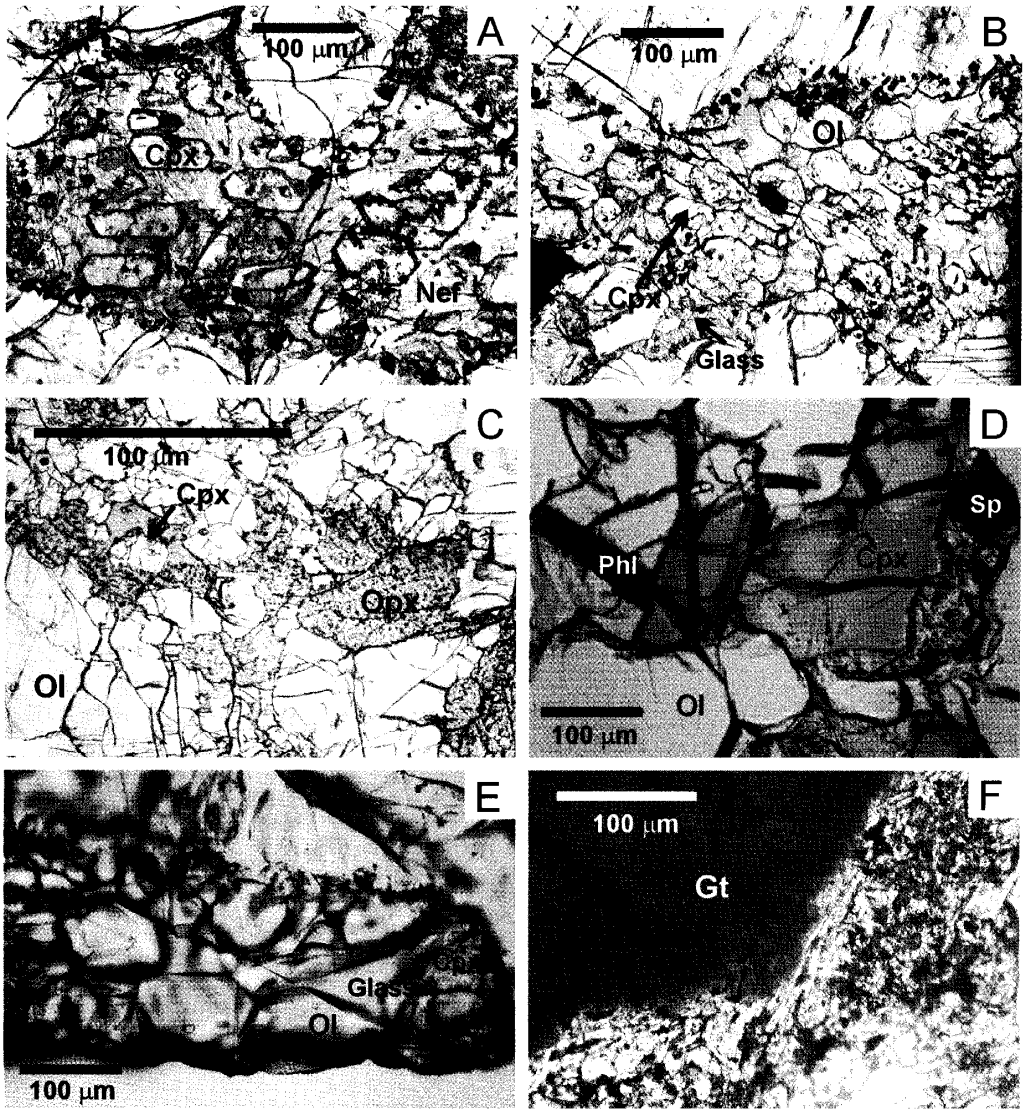

Figure 5. Photomicrographs of Udokan xenoliths. A, euhedral clinopyroxene microlite surrounded by fine Cr-spinel and radial nepheline and leucite in the melt pocket in spinel harzburgite, Ingamakit, sample 106-22. B, similar melt pockets with pink clinopyroxene and euhedral olivine crystals, Ingamakit, sample In-40. C, secondary crystallized pink interstitial clinopyroxene in harzburgite xenolith, Ingamakit, sample 106-16. D, Phlogopite inclusion in melt pocket, sample 106-16. E, melt pockets in spinel lherzolite; Si-rich (70-74 wt.% SiO_2) glass coexisting with olivine microlites, Nizhni Lurbun, sample u19-12. F, secondary assembly near garnet grain in basanite includes leucite, clinopyroxene and altered glass, Kuas, Sample 121-2. Nef, nepheline. See Fig.1 for other abbreviations.

Table 4. Representative analyses (wt.%) of interstitial glasses and melt inclusions in minerals from Vitim xenoliths and host volcanics.

Sample	D-51						D-11						D-82	
	Gt-Sp Lherzolite						Sp Harzburgite						Sp Lherzolite	
Host	ol	ol	opx	opx	cpx	cpx	ol	ol	opx	opx	cpx	cpx		
Type	heat	heat	heat	heat	heat	heat	res	res	res	res	res	res	vein	vein
SiO_2	48.13	48.07	53.89	54.98	55.38	54.93	65.12	65.42	69.92	71.09	70.14	71.13	62.40	63.79
TiO_2	2.56	3.38	1.37	1.28	0.63	0.43	0.26	0.14	0.13	0.12	0.09	0.12	0.42	0.35
Al_2O_3	17.34	17.58	17.28	16.94	17.14	19.70	18.42	19.34	19.01	18.34	16.94	16.35	21.62	18.43
Cr_2O_3	0.02		0.20	0.06	0.21	0.40								
FeO	8.45	5.48	4.05	4.26	3.91	2.26	1.27	1.20	0.92	0.74	0.57	0.59	0.14	0.71
MnO	0.09	0.05	0.07	0.08	0.06	0.06	0.01	0.02	0.12	0.10	0.04	0.05	0.01	
MgO	8.35	7.89	7.45	9.54	6.49	5.74	1.05	0.67	0.59	0.73	0.26	0.39	0.24	1.13
CaO	5.02	7.25	6.09	5.18	8.42	6.53	0.45	0.22	0.36	0.94	1.93	1.79	3.68	1.25
Na_2O	4.45	4.73	4.87	4.62	3.20	5.43	3.66	4.72	3.22	2.71	3.55	5.22	5.60	6.34
K_2O	3.02	2.64	1.84	1.71	1.53	1.14	4.57	4.78	3.32	3.68	2.46	1.81	5.33	7.01
P_2O_5							0.21	0.12	0.35	0.32	0.11	0.35		
Total	97.43	97.07	97.1	98.65	96.96	96.62	95.02	96.63	97.94	98.76	96.09	97.80	99.41	99.01
Mg#	63.8	72	76.6	80	74.7	81.9	59.6	49.9	53.3	63.7	44.8	54.1	75.3	73.9
Alk#	7.5	7.4	6.7	6.3	4.7	6.6	8.2	9.5	6.5	6.4	6.0	7.0	10.9	13.4

Sample	D-3F						D-19					
	Sp Lherzolite						Sp Lherzolite					
Host							opx	opx	cpx	cpx		
Type	vein	vein	mp	mp	rim	rim	heat	heat	heat	heat	vein	vein
SiO_2	60.29	61.01	57.24	55.67	50.87	52.32	52.28	58.06	54.39	56.23	58.79	61.54
TiO_2	0.53	0.56	0.71	0.89	2.13	1.79	0.72	0.97	0.60	0.50	0.85	0.91
Al_2O_3	19.14	17.73	19.12	20.56	18.21	18.76	17.22	17.72	19.05	18.61	24.37	22.59
Cr_2O_3							0.02	0.01	0.03	0.06		
FeO	1.6	1.47	3.3	3.08	6.47	5.91	7.10	5.55	3.96	3.32	1.47	1.62
MnO	0.05	0.01	0.05	0.03	0.09	0.08	0.13	0.10	0.13	0.06		
MgO	1.99	2.43	2.79	2.51	4.12	3.8	8.91	6.00	6.45	5.17	1.89	2.21
CaO	2.21	2.07	3.71	4.12	7.64	7.32	3.02	2.70	4.18	4.92	3.12	2.20
Na_2O	7.02	6.33	6.25	5.56	5.13	4.87	3.96	4.15	5.87	5.53	3.51	4.84
K_2O	6.13	6.71	4.23	5.31	3.79	3.32	2.33	3.33	1.78	2.06	2.56	3.37
Total	98.96	98.32	97.395	97.73	98.45	98.17	95.68	98.6	96.45	96.48	96.56	99.28
Mg#	68.9	74.7	60.1	59.2	53.2	53.4	69.1	65.8	74.4	73.5	69.6	70.9
Alk#	13.2	13.0	10.5	10.9	8.9	8.2	6.3	7.5	7.7	7.6	6.1	8.2

Sample	D-2						BL-32				Ka-2	
	Sp Lherzolite						Gt-Sp Lherzolite				Sp Lherzolite	
Host	Opx	opx	cpx	cpx			gt	gt	gt	gt		
Type	heat	heat	heat	heat	vein	vein	res	res	res	res	vein	vein
SiO_2	52.17	58.7	55.59	58.22	62.38	65.39	52.41	50.44	49.79	51.13	68.01	70.21
TiO_2	5.11	1.68	1.71	0.96	1.41	0.53	0.46	0.51	0.42	0.45	1.28	1.15
Al_2O_3	16.18	16.44	16.72	15.92	11.49	18.51	20.17	21.21	22.13	21.46	19.64	18.67
Cr_2O_3	0.07	0.06	0.30	0.19			0.11	0.09	0.09	0.13		
FeO	4.11	3.17	1.96	1.58	2.38	0.54	4.97	4.48	4.51	3.70	1.46	1.33
MnO	0.06	0.08	0.07	0.06			0.06	0.07	0.05	0.05	0.08	0.02
MgO	9.78	9.26	7.68	5.42	5.43	0.68	5.15	5.81	4.51	5.02	0.55	0.51
CaO	7.81	4.34	9.66	6.57	7.12	2.58	4.79	5.13	5.13	5.17	1.87	1.78
Na_2O	4.33	4.81	5.35	5.81	6.23	3.95	3.23	3.15	3.11	3.89	4.23	3.67
K_2O	0.01	2.62	0.75	2.73	2.59	6.44	4.17	3.67	3.75	4.12	2.25	1.69
P_2O_5							0.12	0.03	0.02	0.02	0.03	0.03
Total	99.63	101.2	99.79	97.46	99.03	98.62	95.64	94.59	93.51	95.14	99.41	99.06
Mg#	80.9	83.9	87.5	85.9	80.3	69.2	64.9	69.8	64.1	70.7	40.4	40.6
Alk#	4.3	7.4	6.1	8.5	8.8	10.4	7.40	6.82	6.86	8.01	6.5	5.4

Table 4, continued

Sample	Ka-101		V-896											
	Sp Lherzolite		Gt Lherzolite											
Host			ol	ol	opx	opx	ol	ol	opx	opx	cp	cp	sp	sp
Type	mp	mp	heat	heat	heat	heat	res	res	res	res	res	res	res	res
SiO_2	58.89	59.41	49.37	50.05	51.03	51.02	52.38	54.00	52.34	55.72	52.70	54.82	51.47	52.14
TiO_2	1.77	1.88	1.17	1.32	1.23	1.44	0.80	0.67	0.81	0.44	0.73	1.01	0.57	0.73
Al_2O_3	18.80	19.13	15.94	16.89	16.01	15.85	17.79	18.78	21.14	21.72	20.31	20.75	21.32	22.55
Cr_2O_3	0.01	0.01	0.17	0.17	0.20	0.21	0.01	0.02	0.05	0.02	0.02	0.01	0.20	0.15
FeO	2.76	2.44	7.79	8.85	7.21	8.02	6.44	5.67	5.13	5.01	5.93	5.79	5.10	4.34
MnO	0.05	0.03	0.07	0.11	0.09	0.09	0.06	0.07	0.05	0.01	0.05	0.03	0.01	0.02
MgO	2.33	1.93	9.21	8.75	9.74	8.94	7.34	6.45	6.85	6.35	5.63	6.31	7.02	7.79
CaO	5.21	4.38	9.42	8.47	8.47	8.79	5.78	5.14	4.55	3.73	5.41	4.13	4.67	4.49
Na_2O	3.70	4.49	2.02	2.63	1.79	2.35	4.05	4.23	4.35	2.97	3.57	2.82	2.73	2.65
K_2O	4.33	5.11	2.44	2.03	2.43	1.95	3.43	2.85	3.13	3.51	3.13	2.93	3.05	2.01
P_2O_5	0.01	0.02	0.12	0.15	0.13	0.14	0.08	0.07	0.05	0.22	0.07	0.11	0.01	0.04
Total	98.10	98.83	97.72	99.42	98.33	98.80	98.16	97.95	98.45	99.70	97.55	98.71	96.15	96.91
Mg#	60.1	58.5	67.8	63.8	70.7	66.5	67	67	70.4	69.3	62.9	66	71	76.2
Alk#	8	9.6	4.5	4.7	4.2	4.3	7.5	7.1	7.5	6.5	6.7	5.8	5.8	4.7

Sample	P-7		V-706		V-99		D-22		K-1		Pc-1		Pc-2	
	Gt pyroxenite		Am-Sp Lher.		Ph Harzburgite		Basanite		Basanite		Picrobasalt		Picrobasalt	
Host							ol*	ol*						
Type	mp	mp	mp	mp	mp	mp	res	res	bg	bg	bg	bg	bg	bg
SiO_2	55.82	56.27	53.68	55.61	63.8	65.12	58.91	59.55	51.72	53.41	57.63	58.82	60.37	60.98
TiO_2	1.19	0.97	2.48	2.57	1.60	0.74	0.72	0.64	1.86	1.15	0.72	0.53	0.79	0.89
Al_2O_3	21.66	21.44	22.56	23.20	17.06	17.27	21.36	23.32	17.11	18.12	23.21	23.84	22.11	22.09
Cr_2O_3	0.10	0.03		0.04					0.02	0.01	0.02		0.01	
FeO	3.72	4.22	3.05	3.01	1.04	0.71	2.57	1.21	9.33	8.58	2.17	2.81	1.77	1.66
MnO	0.10	0.14	0.07	0.05					0.08	0.09	0.13	0.13	0.01	
MgO	2.09	2.02	1.76	2.12	0.25	0.26	1.18	0.49	2.51	1.78	1.13	1.43	1.04	1.15
CaO	5.27	5.51	5.33	4.81	0.30	0.27	4.25	2.30	7.49	5.83	2.11	2.44	2.43	2.47
Na_2O	3.22	2.28	2.50	1.16	4.52	3.91	4.71	5.28	4.01	4.89	5.11	3.00	4.73	4.96
K_2O	2.49	2.20	3.18	1.67	9.44	10.88	5.12	5.56	2.85	4.89	4.37	4.3	4.02	4.19
P_2O_5			0.21	0.28	0.17	0.02					0.31	0.27	0.33	0.40
F			0.20	0.22	0.02	0.03					0.72	0.03	0.31	0.03
Total	95.66	95.07	95.03	94.74	98.20	99.19	98.82	98.35	96.98	98.75	97.63	97.58	97.92	98.82
Mg#	50	46	50.7	55.7	30	39.1	45	41.9	32.4	27	48.1	47.6	51.2	55.3
Alk#	5.7	4.5	5.7	2.8	14	14.8	9.8	10.8	6.9	9.8	9.5	7.3	8.8	9.2

Host, host minerals; vein, interstitial glass in veinlets; mp, glass from melt pockets; rim, glass from xenolith/basalt boundary; res, residual (unheated) melt inclusions; heat, heated melt inclusions; bg, matrix glass in basalt background (K-1, basanite, Kandidushka; Pc-1 and Pc-2, picrobasalt, Bereya Quarry; *, melt inclusions in olivine phenocrysts in host basanite of Dzhilinda. Alk#=Na_2O+K_2O. See table 2 for locations.

Table 5. Representative analyses (wt.%) of interstitial glasses and melt inclusions in minerals from Baikal and Mongolia xenoliths and host volcanics.

Sample	106-26				M-7		u19-12						
	Sp harzburgite				Sp lherzolite		Sp lherzolite						
Host	ol1	ol1	ol2	ol2			ol1	ol1	ol2	ol2			
Type	res	res	res	res	mp	mp	res	res	res	res	mp	mp	mp
SiO_2	64.79	67.50	66.11	70.65	67.34	66.50	72.07	72.19	69.64	70.85	71.26	72.13	73.09
TiO_2	2.50	1.68	1.11	1.06	1.03	0.94	1.07	1.05	0.60	1.14	0.89	0.75	0.87
Al_2O_3	15.88	17.09	11.10	12.79	14.78	15.44	16.09	15.97	13.53	16.68	15.37	14.57	14.22
FeO	3.24	2.62	6.48	2.99	2.14	1.79	1.87	1.80	2.08	1.91	1.92	2.17	2.40
MnO	0.04	0.02	0.06	0.02	0.02	0.02	0.02	0.02	0.01	0.01	0.03	0.03	0.02
MgO	0.89	0.72	5.21	0.96	1.56	1.43	1.13	1.17	1.22	1.06	1.47	1.67	1.61
CaO	0.25	0.11	0.35	0.01	0.88	0.73	0.10	0.11	0.83	0.46	0.06	0.10	0.12
Na_2O	3.64	3.90	2.43	2.97	4.22	3.47	2.11	2.68	2.72	3.15	2.83	1.37	1.38
K_2O	7.56	6.60	5.26	8.19	6.56	7.21	4.24	4.23	6.94	4.57	4.42	3.65	3.86
P_2O_5	0.14	0.12	0.01	0.00	0.12	0.33	0.17	0.20	0.01	0.10	0.43	0.19	0.20
Total	98.93	100.4	98.11	99.64	98.65	97.86	98.87	99.41	97.57	99.93	98.68	96.63	97.77
Mg#	32.9	32.9	58.9	36.3	56.5	58.7	51.9	53.7	51.1	49.7	57.7	57.8	54.5
Alk#	11.2	10.5	7.7	11.2	10.8	10.7	6.4	6.9	9.7	7.7	7.3	5.0	5.2

Sample	74-11				K15		K60	X-06				
	Sp harzburgite				Sp lherzolite		Websterite	Ol websterite				
Host	ol1	ol1									ol1	ol1
Type	res	res	vein	vein	vein	vein	vein	vein	vein	vein	res	res
SiO_2	65.21	66.18	64.33	67.85	53.76	54.41	49.36	50.01	69.72	68.43	64.72	63.15
TiO_2	0.79	0.81	1.27	0.95	0.89	0.74	1.14	1.25	1.07	0.92	0.92	0.86
Al_2O_3	18.25	16.14	18.39	15.72	21.46	21.71	18.59	17.83	14.31	16.86	17.26	17.16
FeO	2.18	2.34	2.14	2.17	2.31	2.17	4.46	4.12	0.95	0.82	1.61	2.86
MnO	0.05	0.05	0.04	0.06	0.03	0.04	0.11	0.06	0.02	0.01	0.03	0.03
MgO	1.26	1.21	1.56	1.61	2.31	2.46	4.54	4.27	0.37	0.36	1.15	2.32
CaO	0.54	0.72	1.12	1.03	2.37	2.55	4.85	4.37	1.43	0.23	1.06	1.65
Na_2O	3.65	3.75	4.12	3.89	8.54	7.82	6.82	6.14	3.35	3.60	4.52	5.25
K_2O	5.89	5.56	3.65	4.37	2.96	2.45	4.00	4.72	5.92	6.75	5.75	3.95
P_2O_5	0.02	0.30	0.12	0.31	0.14	0.10	0.21	0.31	0.12	0.17	0.16	0.21
Total	97.84	97.06	96.74	97.96	94.77	94.45	94.08	93.08	97.26	98.15	97.18	97.43
Mg#	50.7	48.0	56.5	56.9	64.1	66.9	64.5	64.9	41.0	43.9	55.9	59.1
Alk#	9.5	9.3	7.8	8.3	11.5	10.3	10.8	10.9	9.3	10.4	10.3	9.2

Sample	B-002		B-012		B-401		SHT-36		SHT-5		Mo-5a	Mo-5b	Mo-40
	Am-sp wehrlite		Am-sp lher.		Ph-sp lherzolite		Sp lherzolite		Sp lherzolite		[1]	[1]	[1]
Type	mp	mp	mp	mp	mp	mp	mp	mp	mp	mp	mp	mp	mp
SiO_2	51.16	50.23	54.54	54.72	46.71	47.24	53.56	55.89	56.78	61.23	52.96	56.21	61.16
TiO_2	0.51	0.44	1.45	1.37	2.13	2.00	0.55	0.34	0.31	0.27	0.53	0.32	0.39
Al_2O_3	24.36	23.95	23.05	23.60	21.15	22.04	21.12	22.41	21.47	19.34	22.04	23.14	19.49
FeO	2.44	2.07	2.85	2.79	4.03	3.78	2.56	1.89	2.21	1.79	2.35	2.62	2.19
MnO	0.01	0.14	0.07	0.06	0.04	0.05	0.07	0.07	0.04	0.05			
MgO	2.21	1.79	2.41	2.31	3.37	3.51	1.97	1.55	2.17	1.53	2.45	2.13	1.72
CaO	5.91	5.71	5.25	5.64	2.35	2.72	6.89	5.47	4.44	2.46	6.71	4.00	2.75
Na_2O	9.62	9.85	4.13	4.40	5.89	5.87	8.71	9.13	8.31	8.19	10.28	9.82	8.58
K_2O	1.85	2.00	2.45	2.67	7.71	7.23	2.19	1.87	1.85	3.30	0.79	1.31	3.29
P_2O_5	0.87	0.76	0.43	0.46	0.79	0.71	0.73	0.56	0.39	0.21	1.86	0.39	0.36
Total	98.94	96.94	96.63	98.02	94.17	95.15	98.35	99.18	97.97	98.37	100	100	100
Mg#	61.8	60.7	60.1	59.6	59.8	62.3	57.8	59.4	63.6	60.4	65.0	59.1	58.4
Alk#	11.5	11.9	6.6	7.1	13.6	13.1	10.9	11.0	10.2	11.5	11.1	11.1	11.9

[1] data from Ionov et al. (1994). See Table 2 for locations and Table 4 for abbreviations. Ol1, primary olivine of xenolith, ol2, interstitial olivine microlites.

Table 6. Representative analyses of microlites in the intersticies in the Vitim xenoliths and phenocrysts in the host basalts.

Sample	D-82			DY-3F						D-19		
Mineral	ol	plag	ilm	ol	cp	plag	sp	mt	cp	ol	cp	ab
SiO_2	40.83	55.03	0.10	40.34	52.08	55.47	0.14	0.41	50.13	40.21	53.14	63.37
TiO_2	0.01	0.01	51.57	0.02	0.72	0.12	1.24	23.91	1.43	0.05	1.90	0.21
Al_2O_3		27.37	0.11		2.71	28.32	42.58	1.07	3.95		2.02	21.43
Cr_2O_3	0.01		0.72	0.07	0.78	0.01	22.49	0.42	0.41		0.36	
FeO	8.79	0.12	43.75	9.94	3.21	0.07	16.45	70.07	5.78	12.03	3.81	0.22
MnO	0.08		0.44	0.13	0.10		0.17	0.70	0.14	0.23	0.11	0.04
MgO	49.27	0.04	1.74	48.03	17.07	0.08	16.99	1.44	15.00	46.68	15.60	0.54
CaO	0.22	8.38		0.33	20.80	9.01			21.13	0.28	22.46	1.25
Na_2O		6.44			0.51	5.73			0.42		0.34	10.23
K_2O		0.31			0.03	1.05						0.72
NiO	0.25		0.05	0.18			0.27	0.05	0.03	0.15	0.02	
Total	99.46	97.70	98.48	99.04	98.00	99.86	100.3	98.07	98.42	99.63	99.76	98.01
Mg#	90.9			89.6	90.5		64.8		82.2	87.4	87.9	

Sample	DY-8A					B-32			Ka-2		Ka-101		P-7	
Mineral	ol	cp	plag	san	sp	leuc	plag	san	ol	cp	ol	cp	cp	plag
SiO_2	41.44	52.45	55.34	64.84	0.18	55.97	58.59	65.40	41.28	50.54	41.22	53.88	51.67	55.27
TiO_2	0.05	1.23	0.49	0.76	3.71	0.07	0.16	0.57		1.14	0.01	0.49	0.62	0.22
Al_2O_3		3.43	25.77	18.43	44.62	23.10	25.70	20.60		6.80		1.22	4.36	26.30
Cr_2O_3	0.01	0.81		0.02	26.37				0.06	0.99		1.13	2.05	
FeO	6.59	1.91	0.31	0.12	12.21				9.67	3.80	8.03	2.28	3.01	0.21
MnO	0.12	0.08	0.02		0.08				0.19	0.12	0.04	0.07	0.08	
MgO	51.48	14.24	0.58	0.04	11.78	0.04	0.02	0.06	49.06	15.42	50.50	17.23	15.75	0.13
CaO	0.15	22.45	9.05	0.45			7.04	1.40	0.14	19.11	0.21	21.59	21.47	9.62
Na_2O		0.75	5.61	5.14		0.01	6.65	5.77		1.18		0.85	0.79	5.79
K_2O		0.01	0.40	8.79		19.98		4.50		0.02				0.42
NiO	0.21				0.22				0.31	0.05	0.22			
Total	100.1	97.34	97.57	98.59	99.17	99.18	98.16	98.29	100.7	99.15	100.2	98.74	99.80	98.00
Mg#	93.3	93.0			63.2				90.0	87.9	91.8	93.1	90.2	

Sample	V-706			D-1*						K-1*		Pb-1*			
Mineral	ol	cp	cp	ol	cp	cp	mt	pl	ab	ol	cp	ol	op	cp	sp
SiO_2	40.95	44.73	49.10	38.86	46.26	49.11	0.06	54.21	51.14	38.43	48.99	39.11	50.14	46.81	0.10
TiO_2	0.02	3.91	1.61		3.53	2.21	25.27	0.14	0.05	0.09	2.55	0.02	0.11	0.45	6.80
Al_2O_3	0.01	9.16	5.90	0.03	7.41	4.63	2.18	29.30	29.11	0.07	5.13	0.03	11.44	14.46	11.28
Cr_2O_3	0.04	0.75	1.05	0.03	0.05	0.11	0.26	0.01	0.07	0.04	0.01	0.05	0.97	0.89	18.51
FeO	7.81	3.49	2.79	21.00	8.00	7.85	67.55	0.51	0.97	21.87	8.41	17.58	7.45	3.92	55.83
MnO	0.09	0.05	0.06	0.35	0.11	0.21	0.67	0.06		0.35	0.12	0.21	0.48	0.38	0.76
MgO	49.74	13.52	15.28	40.18	11.37	13.43	2.15	0.07	0.19	38.53	12.26	42.05	26.79	13.24	4.55
CaO	0.17	22.16	21.78	0.22	22.20	21.20	0.15	11.13	0.06	0.50	21.89	0.43	2.09	18.67	0.31
Na_2O	0.02	0.70	0.55	0.01	0.45	0.33		5.07	16.49		0.57		0.06	0.30	0.08
K_2O	0.01	0.01	0.03	0.01	0.03	0.01		0.33	1.57	0.02	0.02	0.01			
NiO				0.19		0.01			0.06	0.17	0.01	0.15			
Total	98.85	98.47	98.15	100.9	99.40	99.10	98.29	100.8	99.71	100.1	99.96	99.64	99.52	99.12	98.21
Mg#	91.9	87.4	90.7	77.3	71.7	75.3				75.8	72.2	81.0	86.5	85.7	12.7

*, minerals from basanite (D-1, K-1) and picrobasalt (Pb-1) backgrounds. Plag, plagioclase; ilm, ilmenite; mt, magnetite; ab, albite; san, sanidine; leuc, leucite. See table 2 for other abbreviations and sample locations.

Table 7. Representative analyses of microlites in the intersticies in the Udokan xenoliths and phenocrysts in the host basalts.

Sample	In-40									106-16				
Mineral	cp	cp	cp	sp	sp	ol	ol	leuc	nef	cp	cp	sp	ol	ol
SiO_2	55.40	51.54	49.10			38.68	40.61	54.74	44.78	47.72	50.99		41.33	40.51
TiO_2	0.01	1.06	3.61	0.37	3.88	0.01				1.14	0.63	0.43	0.01	0.01
Al_2O_3	0.94	1.79	2.27	5.86	15.61			23.70	33.60	8.63	5.07	38.30	0.01	0.01
Cr_2O_3	1.07	1.03	0.59	55.62	41.45					2.67	1.78	26.92		
FeO	2.71	2.36	4.33	26.49	25.17	16.25	10.09	0.11	0.39	2.40	1.96	18.06	9.08	12.31
MnO	0.10	0.05	0.29	0.16	0.21	0.26	0.18			0.04	0.04	0.17	0.12	0.20
MgO	17.01	16.71	15.98	10.00	12.16	43.17	48.09	0.01	0.04	13.58	15.78	14.83	48.28	45.70
CaO	21.67	23.10	23.39	0.01	0.04	0.54	0.26	0.03	0.53	22.62	22.03	0.08	0.30	0.47
Na_2O	1.20	0.55	0.66					0.63	16.63	0.58	0.65			
K_2O		0.01	0					19.83	4.17					
NiO				0.14	0.29	0.31	0.32					0.20	0.36	0.28
Total	100.1	98.20	100.2	98.65	98.81	99.22	99.55	99.04	100.1	99.38	98.93	99.00	99.49	99.49
Mg#	91.8	92.7	86.8	40.2	46.3	82.6	89.5			91.0	93.5	59.4	90.5	86.9

Sample	106-22					N2-1					74-24			
Mineral	cp	sp	sp	ol	leuc	san	cpx	cpx	ol	mt	cpx	plag	ol	sp
SiO_2	48.05			41.25	55.20	65.34	48.93	49.90	40.90		49.27	54.87	41.09	0.09
TiO_2	0.91	0.44	0.41				3.57	1.31	0.01	14.19	0.30	0.10		0.11
Al_2O_3	8.27	49.33	45.23		23.29	18.11	3.71	4.81	0.01	1.88	7.60	26.13	0.13	45.86
Cr_2O_3	2.06	17.66	22.25				0.24	1.75		0.01	2.93	0.18	0.08	21.60
FeO	2.79	13.62	11.69	8.31	0.13	0.42	5.43	3.23	10.63	76.99	2.63	0.36	8.03	9.97
MnO	0.00	0.17	0.12	0.12	0.00	0.00	0.24	0.17	0.14	1.12	0.06		0.15	0.15
MgO	14.38	18.20	18.60	49.81	0.03	0.06	14.21	15.75	46.97	2.68	14.52	0.26	50.14	21.75
CaO	22.04	0.32	0.01	0.24	0.15	0.05	21.56	21.01	0.31	0.11	23.24	8.96	0.39	0.03
Na_2O	0.63				0.12	4.59	0.85	1.12			0.37	6.30	0.02	
K_2O					20.91	10.30	0.01				0.01	0.47	0.01	
NiO		0.25	0.22	0.34					0.31					
Total	99.13	99.98	98.53	100.1	99.83	98.87	98.75	99.05	99.28	96.97	100.9	97.61	100.0	99.54
Mg#	90.2	70.4	73.9	91.4			82.3	89.7	88.7	5.8	90.8	56.7	91.8	79.5

Sample	121-2					106-23*					u19-12*			
Mineral	kel	cp	s p	ol	plag	san	ol	mt	leuc	nef	cp	c p	ol	ol
SiO_2	38.83	45.13		39.36	49.95	65.54	37.56		55.95	43.57	48.83	46.83	38.32	38.39
TiO_2	0.00	4.22	0.21	0.00			0.03	21.37			1.98	2.41	0.023	0.031
Al_2O_3	19.72	6.42	64.70	0.04	31.14	19.62	0.01	1.64	23.53	33.23	5.00	7.21	0	0
Cr_2O_3	0.08	0.03	0.14					0.41			0.21	0.43	0.003	0.009
FeO	13.89	7.83	15.97	14.22	0.47	0.22	22.84	71.08	0.29	0.74	5.89	6.36	20.37	22.19
MnO	0.63	0.11	0.40	0.34	0.00	0.00	0.44	0.60	0.00	0.00	0.06	0.09	0.409	0.495
MgO	21.17	12.68	18.95	44.62	0.06	0.01	37.51	2.78	0.05	0.05	14.28	13.24	39.9	37.97
CaO	4.80	22.09	0.01	0.19	14.24	1.33	0.57	0.02	0.06	0.81	22.73	22.28	0.675	0.75
Na_2O	1.67	0.60			3.28	4.93			0.13	16.77	0.53	0.64		
K_2O	0.14	0.00			0.22	8.98			20.13	4.46				
NiO			0.05	0.10			0.15	0.10					0.128	0.091
Total	100.9	99.10	100.4	98.86	99.35	100.6	99.10	97.99	100.1	99.63	99.51	99.49	99.83	99.93
Mg#	73.10	74.27	67.90	84.83			74.54	6.52			81.21	78.77	77.7	75.3

*, minerals from host melaleucitite background. Plag, plagioclase; mt, magnetite; san, sanidine; leuc, leucite; nef, nepheline; kel, kelyphite after garnet. See table 2 for other abbreviations and sample locations.

feldspatic minerals, like plagioclase, sanidine, leucite etc. Rarely, mica, rhonite, Fe-Ti-oxides (like ilmenite, rutile and armalkolite) and sulfide minerals can also be found in melt pockets. Carbonate is not typical for Baikal xenoliths and if it occurs it can represent secondary alteration. Composition of major minerals from melt pockets is usually similar for all localities. Typically, olivine and clinopyroxene have high Mg# number of 91-95 and spinel contains 21–26 wt.% Cr_2O_3. Composition of feldspars and feldspathoids varies widely from plagioclase to K-rich sanidine and leucite (Fig.6). Selected microlite compositions are shown in Tables 6-9.

8.1. Vitim field

Melt pockets in Vitim xenoliths contain clinopyroxene, olivine, and Cr-spinel microlites. Olivine has high Mg#=87–93 and contain CaO=0.2–0.4 wt.%. Clinopyroxene has Mg#=88–94 and has high Cr_2O_3 (up to 2.1 wt.%), CaO, and low Al_2O_3 (1.2–5.0 wt.%) and Na_2O (0.3-1.0 wt.%) relative to primary clinopyroxene in xenoliths (Fig.7). In some cases, however Al_2O_3 in microlite clinopyroxene is 8-10 wt.% (e.g. Ka-103). Clinopyroxene in melt pockets around amphibole in V-706 also has high Al_2O_3 (up to 10 wt.%) and TiO_2 (up to 4.1 wt.%) (Fig.7, Table 3). Spinel contain Cr_2O_3 22–32 wt.% and has Mg#=47–63. Plagioclase of microlites and melt inclusions in Dzhilinda clinopyroxenes has composition of $An_{40\text{-}50}Ab_{50\text{-}60}$. Plagioclase from primary melt inclusions in orthopyroxene (reported by Litasov *et al.*, 2003b) is Ca-rich and contain significant amount of FeO and MgO. These inclusions possibly represent the former glass, but clearly correspond to the plagioclase stoichiometry.

8.2. Udokan field

Melt pockets are very abundant in harzburgite xenoliths from melanephelinite volcanoes of Udokan volcanic field. The interstices in these xenoliths are filled with the following assemblages: (1) olivine + Cr-clinopyroxene + Cr-spinel + sulfides + glass (or sanidine, leucite); (2) olivine + ilmenite + rhonite ± Ba-Ti-mica + leucite, and (3) association similar to meleleucitite groundmass. The presence of the reaction rims is typical of some primary xenolith minerals. The essential phases (olivine, clinopyroxene) of the interstitial associations drastically differ in chemistry from primary xenolith minerals and approach the central zones of melanephelinite phenocrysts or tend to extremely depleted (Mg#>92) and Cr-rich compositions. Consequently, we can observe two trends of clinopyroxene compositions: (1) toward clinopyroxene in host meleleucitites; (2) toward metasomatic enrichment by Cr and Al (Fig.7). First type of clinopyroxene occurs as pink grains between primary minerals and sometimes as subhedral grains in melt pockets (Fig.5B–C) and second type occurs as euhedral crystals in melt pockets (Fig.5A).

Unique Ba-Ti-micas (phlogopite in the xenoliths and biotite in host volcanics) are usually presented in Udokan samples (Table 8). These micas containing 6.5–9.0 wt.% BaO and 11-13 wt.% TiO_2 were not described in other localities worldwide.

8.3. South Baikal and Mongolia

Many Hamar-Daban xenoliths contain melt pockets and interstitial materials. Similar melt pockets are rarely observed in Sayan xenoliths. Ionov *et al.* (1995) described melt

pockets in spinel lherzolites of Hamar-Daban consist of different feldspar, and minor clinopyroxene, Cr-spinel, sulfide, ilmenite, and rutile. Thin interstitial feldspar veinlets were less common. The composition of feldspar in the Hamar-Daban xenoliths varies from plagioclase (An_{50}) trough Ca-anorthoclase to anorthoclase and sanidine (Fig.6).

Amphibole-bearing spinel lherzolite from Bartoy volcanics often contain melt pockets and glass around amphibole, clinopyroxene, and spinel grains (Litasov *et al.* 2000d). Interstitial assemblages consist of glass, olivine, spinel and clinopyroxene (Fig.4H). Secondary olivine is characterized by high Mg# (91.5–94.0) and CaO (0.21–0.28 wt.%). Spinel is generally similar to primary one. Glasses have high Na_2O (9–10 wt.%) and P_2O_5 (0.7–1.7 wt.%).

Burkal spinel and garnet-spinel lherzolite often contain veinlets with minerals corresponding to the host melanephelinites. Some spinel lherzolites include symplectite-like aggregates between orthopyroxene and olivine grains (Fig.8). These aggregates consist of clinopyroxene, olivine, and sanidine (Table 9). Clinopyroxene has Mg#=90–94 and contain 0.2–0.3 wt.% TiO_2 and 0.4–1.2 wt.% Al_2O_3 (Fig.7). Olivine has Mg#=88–90 and contain 0.12–0.17 wt.% CaO. Calculated bulk compositions of the symplectites do not correspond to any mineral observed in mantle xenoliths from basalts (Table 10, see section 9.2).

9. Discussion

9.1. The depth of trapping

Pure CO_2 compositions of fluid inclusions in Baikal xenoliths are comparable to those hosted in minerals of many other ultramafic xenolith suites (Roedder, 1965; Murck *et al.*, 1978; Solovova *et al.*, 1982; Frezotti *et al.*, 1991; 1994; Schiano *et al.*, 1994; Szabo *et al.*, 1996; Ertan and Leeman, 1999). Coexistence of CO_2-rich fluid with silicate melt inclusions strongly implies that fluid in Vitim xenoliths were associated with trapped melts. We suggest that high density CO_2 was separated to fluid phase while H_2O and possibly other volatiles were taken up by silicate melt. This is supported by experimental studies of CO_2 solubility in silicate melt at 1-15 kbar (Roedder, 1965; Spera and Bergman, 1980), system peridotite + CO_2 (Wallace and Green, 1991), and data for other suites (e.g. Szabo and Bodnar, 1996; Ertan and Leeman, 1999).

Using temperature estimates for melt inclusions and density for CO_2-fluid inclusions, it is possible to specify minimum pressure (depths) of inclusion entrapment and P-T ascent paths of mantle xenoliths (Fig.9). For the garnet lherzolite from Bereya Quarry (Vitim field) the density of inclusions (1.12–1.17g/cm^3) records entrapment at minimum pressures of about 13–16 kbar (43–53 km). This is consistent with previous estimations of Schiano and Clocchiatti (1994) for Vitim xenoliths, but is extended to the higher pressures and can be considered as one of the deepest estimations for fluid inclusions in alkaline basaltic xenoliths (Fig.9A). The density of CO_2 inclusions and therefore depth of trapping in other Vitim locations is different. The density of CO_2 inclusions in one of the Kandidushka xenolith is even higher (1.18g/cm^3), however estimated minimal pressure of entrapment is a little lower (13–14 kbar) according to low homogenization temperatures of melt inclusions. For the Dzhilinda lherzolites the highest density of inclusions is 0.94-0.99 g/cm^3, corresponding to the entrapment pressures of 8-10 kbar.

The density of CO_2 inclusions in Udokan xenoliths (1.0–1.05 g/cm^3) correspond to the pressures of 8–10.5 kbar. For Bartoy lherzolites the highest density of inclusions is

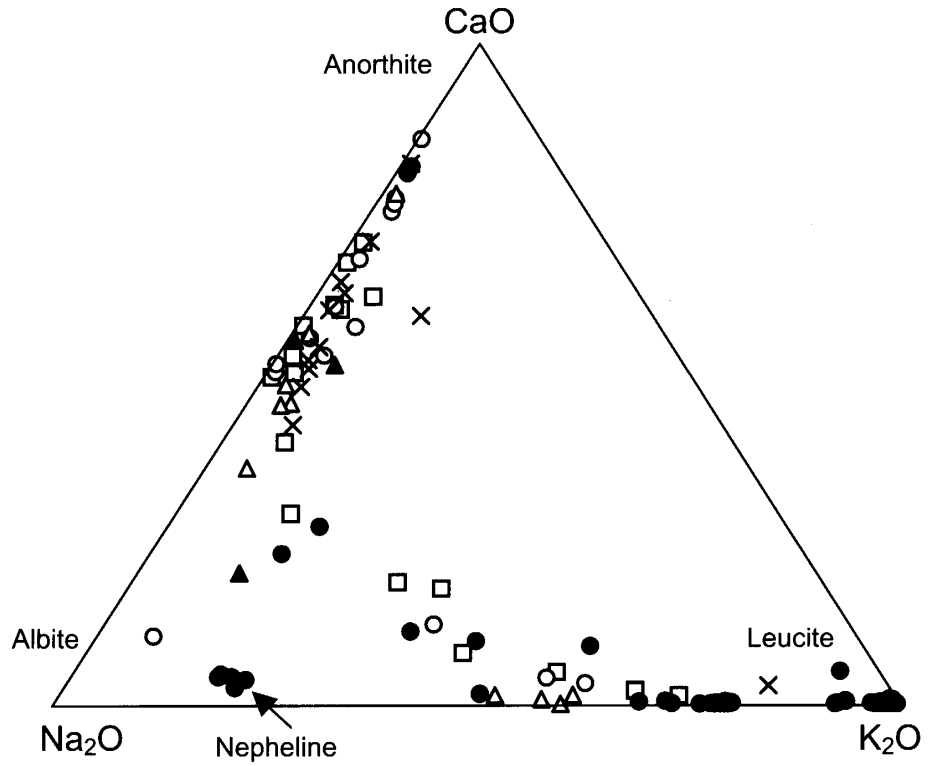

Figure 6. Feldspar and feldspathoid compositions from microlites in Baikal xenoliths in the diagram Na_2O-CaO-K_2O. Open circles, Vitim field; *filled circles*, Udokan filed; *open squares*, Hamar-Daban; *filled triangles*, Sayan; open triangles, Burkal. *Crosses*, compositions of plagioclase from lower crust xenoliths of the Vitim field.

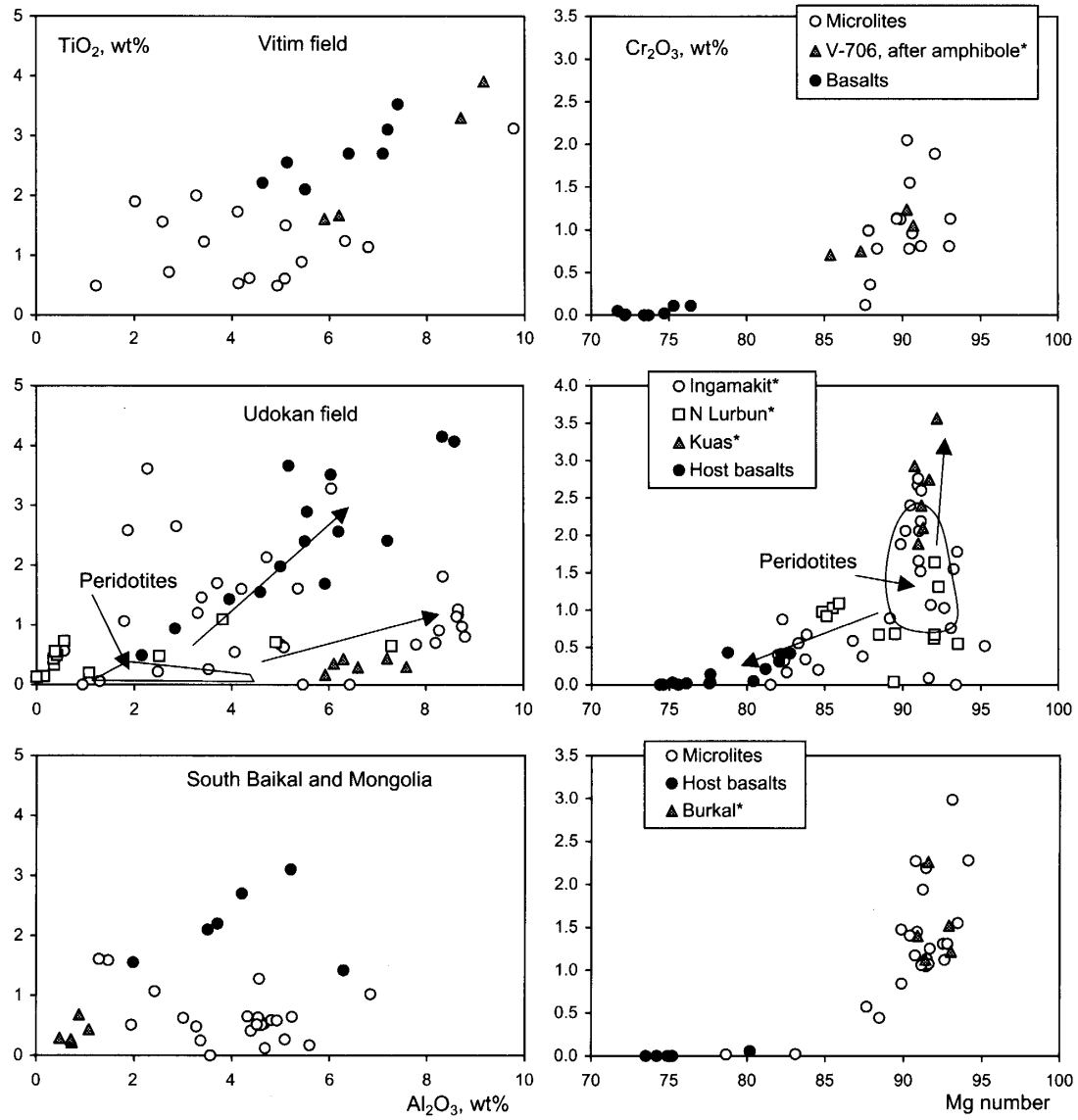

Figure 7. Composition of clinopyroxene microlites in Baikal xenoliths. Compositional fields of depleted peridotite of Northern Udokan and two different trends of metasomatic enrichment of microlites are shown. *, microlites, if not specified.

Table 8. Composition of Ba-Ti-micas from xenoliths and host melaleucitites of Ingamakit volcano, Udokan field.

Sample	In-40		106-16	106-23*
SiO_2	33.41	33.30	33.45	31.05
TiO_2	11.63	12.72	11.37	12.18
Al_2O_3	13.27	13.13	13.61	12.99
Cr_2O_3	0.37	0.28	0.28	0.24
FeO	8.04	9.92	6.07	11.90
MnO	0.12	0.21	0.13	0.19
MgO	14.34	14.01	15.8	11.17
CaO	0.12	0.39	0.37	0.19
NiO	0.13	0.16	0.20	0.09
BaO	6.86	6.60	7.66	9.12
SrO	0.04		0.10	
Na_2O	0.84	0.70	0.70	0.82
K_2O	6.49	7.12	6.60	5.71
F	1.88	1.16	1.82	1.83
Total	97.55	99.70	98.14	97.46
Mg#	76.1	71.6	82.3	62.6

*, biotite from host melaleucitite background

Table 9. Representative analyses of microlites in the intersticies in the Baikal and Mongolia xenoliths and phenocrysts in the host basalts.

	Sayan			Hamar-Daban								Bartoy			
Sample	K-60	K-60	K-101	X-13		X-24	X-6	X-69*		X-13*		B-002			
Mineral	cp	plag	cp	cp	plag	san	cp	plag	san	plag	san	cp	sp	ol	fas
SiO_2	51.95	57.88	52.72	51.83	56.63	66.30	53.13	56.19	65.60	55.85	63.89	50.85	0.07	40.56	44.03
TiO_2	0.41	0.09	0.25	0.64	0.30	1.09	1.07	0.31	0.24	0.20	0.23	0.51	0.33	0.02	1.87
Al_2O_3	4.39	25.00	3.36	5.23	25.46	18.73	2.41	26.43	18.35	26.14	20.22	4.61	42.76	0.03	14.22
Cr_2O_3	1.45		1.25	1.07			0.57	0.11	0.04			1.55	22.82	0.16	0.07
FeO	3.02	0.20	2.76	2.68	0.38	0.49	4.40	0.20	0.13	0.22	0.19	2.07	10.44	7.03	3.48
MnO	0.10	0.15	0.10	0.07	0.12		0.14					0.04	0.16	0.13	0.09
MgO	16.82	0.33	17.06	16.40	0.12	0.29	17.50				0.03	16.56	20.09	51.08	11.36
CaO	21.16	7.89	21.38	21.04	8.01	0.20	20.20	9.39	0.19	9.65	2.56	22.19		0.24	22.08
Na_2O	0.55	6.41	0.50	0.61	6.99	2.92	0.45	5.78	3.89	5.93	6.73	0.50			0.61
K_2O		1.08			0.21	6.52	0.06	0.56	11.20	0.40	5.39				0.16
NiO				0.11			0.13					0.02	0.28	0.29	
Total	99.84	99.03	99.37	99.68	98.26	96.83	100.1	98.97	99.64	98.39	99.24	98.90	97.19	99.54	97.98
Mg#	90.9		91.7	91.6			87.6					93.5	77.5	92.8	85.3

	Bartoy			Burkal								Shavaryn-Tsaram			
Sample	B-012			Bu-15		Bu-11			Bu-30			SHT-36		SHT-5	
Mineral	cp	ol	sp	cp	plag	ol	cp	san	ol	cp	san	cp	ol	cp	ol
SiO_2	51.34	40.70	0.11	51.84	55.97	41.05	54.32	66.98	41.08	54.72	65.98	52.67	41.14	53.89	40.99
TiO_2	0.58	0.03	2.12	0.27	0.01	0.04	0.43	0.40	0.04	0.29	0.14	0.48		0.51	
Al_2O_3	4.92	0.01	43.79	5.08	26.70		1.08	19.08	0.01	0.48	19.05	3.27		1.94	
Cr_2O_3	1.31	0.05	24.64	1.31	0.04	0.01	2.26		0.06	1.22	0.08	2.19		1.12	
FeO	2.38	9.10	11.43	2.15	0.21	11.21	2.82	0.56	9.11	2.39	0.64	2.63	7.89	2.50	6.75
MnO	0.06	0.12	0.12	0.07		0.13	0.06		0.05	0.11		0.11	0.11	0.08	0.07
MgO	16.48	49.78	16.08	15.52	0.02	48.92	17.21	0.03	49.48	17.81	0.15	15.74	50.53	17.55	50.94
CaO	21.62	0.17		22.21	8.64	0.15	20.80	0.11	0.13	21.41	0.18	21.57	0.21	20.87	0.19
Na_2O	0.56	0.01		0.38	6.53	0.01	0.69	6.02		0.52	6.53	0.95		1.02	
K_2O					0.25		0.01	8.14		0.02	7.04				
NiO	0.07	0.27	0.26	0.08		0.27	0.03	0.02	0.18	0.08			0.28		0.31
Total	99.29	100.2	98.55	98.91	98.38	101.7	99.71	101.3	100.1	99.05	99.78	99.61	100.2	99.48	99.25
Mg#	92.5	90.7	71.5	92.8		88.6	91.6		90.6	93.0		91.4	91.9	92.6	93.1

*, Data from Ionov et al., 1995. Plag, plagioclase; san, sanidine; fas, fassaite. See table 2 for other abbreviations and sample locations.

Table 10. Calculated bulk composition of clinopyroxene-olivine-sanidine symplectites from Bartoy peridotites (Fig.8).

Sample	Bu-11	Bu-100	Bu-30	Bu-16
SiO_2	49.27	49.93	49.49	50.17
TiO_2	0.27	0.29	0.19	0.20
Al_2O_3	1.01	1.06	0.66	0.69
Cr_2O_3	1.31	1.43	0.73	0.79
FeO	6.13	5.71	5.04	4.71
MnO	0.09	0.08	0.08	0.09
MgO	29.55	27.96	30.12	28.54
CaO	12.13	13.16	12.47	13.54
Na_2O	0.52	0.56	0.43	0.46
K_2O	0.17	0.17	0.15	0.15
NiO	0.13	0.11	0.12	0.11
Total	100.5	100.4	99.48	99.43

Figure 8. Back-scattered electron image of clinopyroxene-olivine-sanidine symplectites in the peridotite xenolith from the Burkal melaleucitite. Sample Bu-16. Scale bar 100μm.

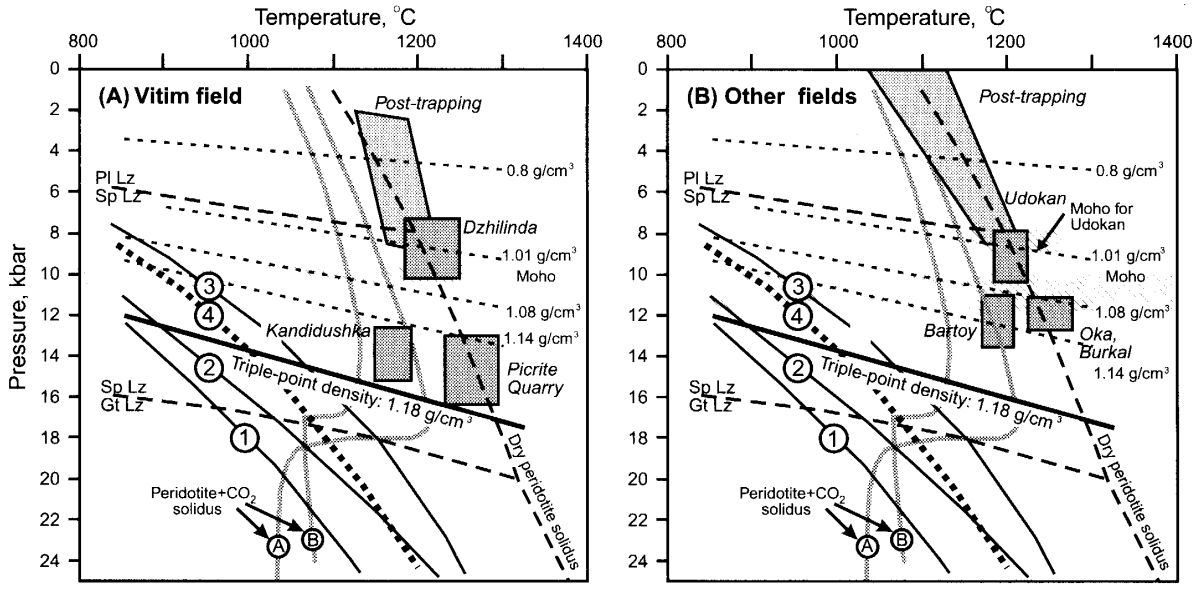

Figure 9. Limited pressure and temperature conditions for fluid and melt inclusions trapping in mantle xenoliths from the Baikal volcanics. Boxed of trapping conditions have been estimated from T-density data for fluid and melt inclusions. Dotted lines, different isochors for pure CO_2 with the indicated densities (Andersen and Neumann, 2001), calculated using equation of state of Holloway (1981), which is consistent with those of Bottinga and Richet (1981) used in our calculations. Dashed lines are transition boundaries between fertile plagioclase, spinel and garnet lherzolite (Mg#=90 and Cr#Sp=10 (O'Neill, 1981; Herzberg, 1978; Gasparik, 1984) and solidus of dry lherzolite (Takahashi and Kushiro, 1983). Grey lines are solidi of (A) peridotite+CO_2 (Wyllie, 1978; Green and Fallon, 1998) and (B) peridotite+CO_2+H_2O (Olafsson and Eggler, 1983). Numbered lines are geotherms based on xenolith mineral thermobarometry (1-3, Vitim volcanic fields: (1) garnet lherzolites from Miocene picrobasalts, (2) garnet lherzolites from Pliocene basanites, (3) Al-augute garnet pyroxenites from Miocene picrobasalts (Litasov *et al.*, 2000c), (4) reference South-Eastern Australia geotherm (O'Reilly and Griffin, 1985) resemble to geotherms of South Baikal (Sayan, Hamar-Daban, and Bartoy, Litasov and Taniguchi, 2002). Moho boundary is after Zorin *et al.* (1989) and Litasov and Taniguchi (2002).

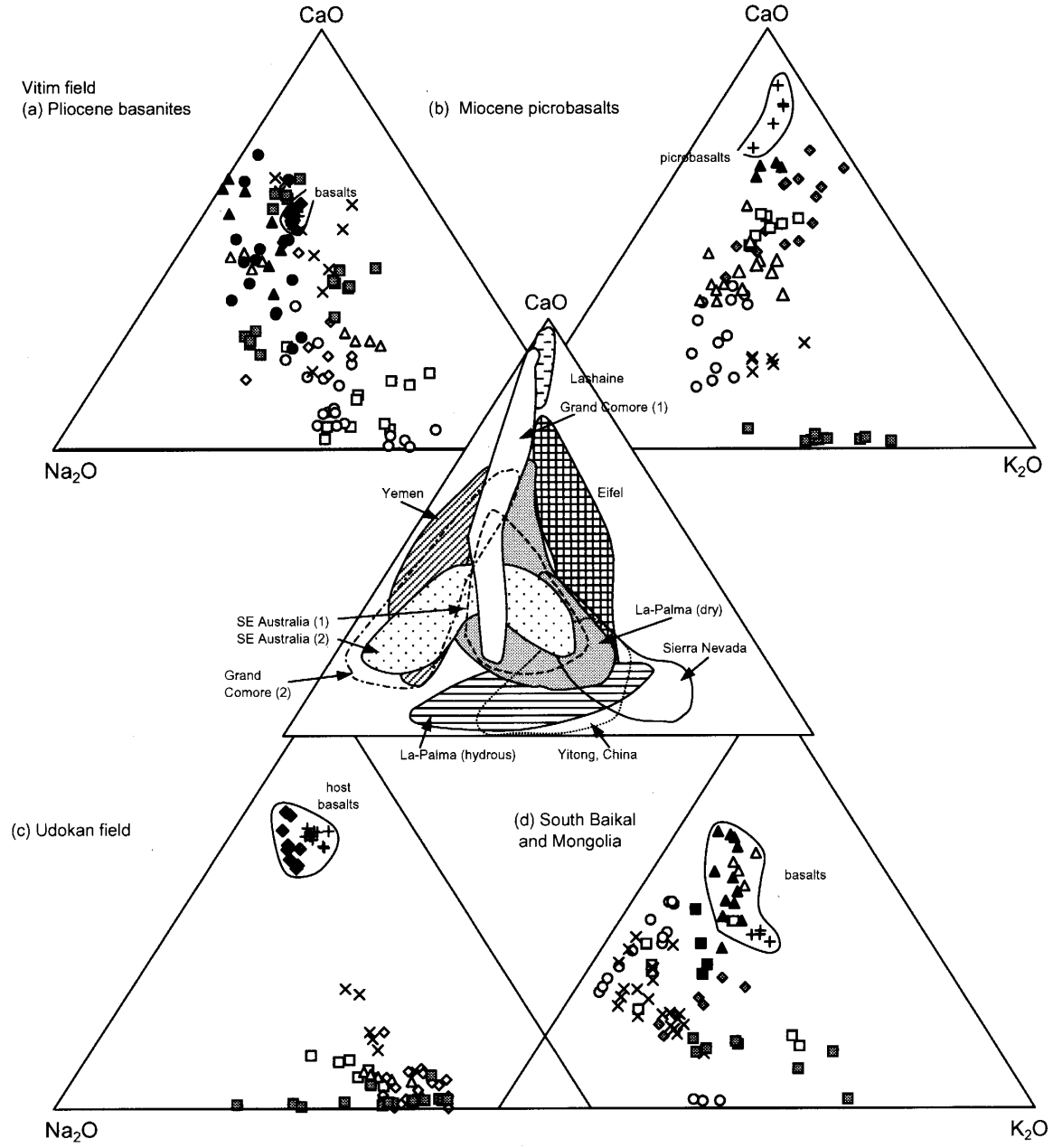

Figure 10. Comparison of glass compositions from Baikal and Mongolian xenoliths and glass from other world locations in the diagram Na_2O-CaO-K_2O. Symbols are same as in Fig.2 and 3. World data: La-Palma, "dry" and "hydrous", anhydrous and amphibole-phlogopite-bearing peridotites (mainly harzburgites) from La Palma, Canary (Newmann and Wulff-Pedersen, 1997); Grand Comore (1), compositional trend of glasses of primary inclusions in minerals of single spinel lherzolite of Grand Comore Island, Comores (Schiano *et al.*, 1998); Grand Comore (2), carbonated spinel lherzolites of Grand Comore Island, Comores (Coltorti *et al.*, 1999); Lashaine, garnet spinel lherzolite from Lashaine volcano, Tanzania (Schiano *et al.*, 2000); Eifel, peridotite from Gees, West Eifel, Germany (Zingrebbe and Foley, 1995); Yemen, Amp-bearing lherzolites from Southern Yemen (Chazot *et al.*, 1996); SE Australia (1), lherzolites, harzburgites, and amphibole-phlogopite-apatite wehrlites from Western Victoria, Australia (Varela *et al.*, 1999); SE Australia (2), metasomatized peridotites from Newe field, southeastern Australia (Yaxley and Kamenetsky, 1997); Yitong, wehrlites from Yitong, northeastern China (Xu *et al.*,1996); Sierra Nevada, spinel lherzolites from Sierra Nevada, California (Ducea and Salleby, 1998).

1.16g/cm^3. According to T_{hom}=1150−1200℃ minimum entrapment pressures can be estimated as of 12-14 kbar. Pressure range for CO_2 inclusions from Burkal xenoliths is similar (Fig.9B). Estimated depth of trapping for Udokan, Bartoy and Burkal xenoliths (Fig.9B) are well correlated with the depth of Moho estimated from seismological and petrological data (Zorin *et al.*, 1989; Litasov and Taniguchi, 2002).

Estimated CO_2-pressures for Dzhilinda xenoliths in Vitim are considerably lower than those for xenoliths from Kandidushka and Bereya Quarry. This difference can be attributed to re-equilibration of CO_2 inclusions resulting from the delay during transport to the surface or change in the ascent rate of the xenoliths (Frezotti *et al.*, 1994; Szabo and Bodnar, 1996). Possible change in ascent rates for xenolith-bearing magmas near crust/mantle boundary were proposed by Griffin *et al.* (1984) for Bullenmerri and Gnotuk suites, SE Australia (~0.1 m/s below 10 kbar and ~10 m/s above 10 kbar) and Szabo and Bodnar (1996) for Nograd-Gomor volcanic field, Hungary/Slovakia. Above the critical depth magma ascent is driven by the mechanics of crack propagation governed by the boiling and liberation of volatiles from the magma (Griffin *et al.*, 1984). This mechanism and possible delay at the uppermost mantle level or change of ascent rate near Moho is very likely to be applied for the Dzhilinda xenoliths. The suite contains abundant garnet lherzolite (series 1, see section 4) but almost all garnets have been replaced by kelyphite aggregates and clinopyroxene has thick spongy rims in these samples. Thus, replacement of garnet and re-equilibration of CO_2 inclusions in series 1 peridotites can be resulted from the same process described above. Similar mechanism is also applicable for Northern Udokan, where possible delays of magma at the crust-mantle boundary are detected by abundant melt pockets as evidence for partial melting of xenoliths.

9.2. The origin of glasses and microlite minerals

A triangular plot of Na_2O, CaO, and K_2O can be used to compare the chemistry of the glasses in mantle xenoliths from different localities. The glasses from xenoliths in Pliocene basanites of Vitim field define an elongated field in this triangle (Fig.10a) stretching parallel to CaO−K_2O join. Unheated inclusions and interstitial glasses fall into K-rich part of this trend, while heated inclusions are CaO-rich. The glasses from xenoliths in Miocene picrobasalt of the Vitim field define field stretching parallel to CaO-Na_2O join except glasses from V−99 formed by phlogopite melting (Fig.10b). Glasses from Vitim xenoliths cover most of fields observed for many literature data worldwide. Therefore, variations of glass compositions should be addressed to various processes taking place in the mantle or during transport of xenoliths to the surface.

The glasses from Udokan xenoliths vary along Na_2O-K_2O join and extremely CaO-poor (Fig.10c).

These features can be attributed to host K-Na-rich melaleucitite/melanephelinite lavas. Most glasses from Mongolian xenoliths define field along CaO-Na_2O join, whereas those from South Baikal tend to be K_2O-rich (Fig.10d).

Glass in mantle xenoliths may originate by many different processes (see reviews by Newmann and Wulff-Pedersen, 1997; Draper and Green, 1997; Shaw *et al.*, 1998). The hypotheses for origin of the intraxenolith glasses can be summarized as follows: (1) infiltration of host basalt magma or related fluid during transport to the surface, reaction between infiltrating basaltic melts and peridotite (Zingrebbe and Foley, 1995; Wulff-

Pedersen *et al.*, 1996); (2) breakdown of mantle minerals (typically amphibole) in response to decompression (Frey and Green, 1974; Francis, 1976) or partial melting of xenolith's minerals in response to heating by the host lava (Klugel, 1998) during ascent to the surface; (3) in situ interaction of melt/fluid and mantle minerals prior to transport of xenoliths to the surface (Ionov *et al.*, 1994); (4) in situ partial melting involving breakdown of primary xenolith's minerals (Francis, 1987; Chazot *et al.*, 1996). The following peculiarities of different hypotheses are addressed to specify which minerals melting or what kind of melt/fluid react with peridotite.

In many cases, glasses in mantle xenoliths results from their interaction with melt or fluid genetically related to the host volcanic rocks (this is clear for example for Udokan xenoliths). However, determination of depth for origin of the glasses is very difficult. We can determine pressure directly from fluid inclusions in microlite minerals grown from intergranular melt, but they are typically very small or absent. For instance CO_2 in fluid inclusions in olivine microlites from Udokan harzburgites has density of 0.7–0.9 g/cm^3 indicating their growth during transportation to the surface.

Some glasses presented in this study are clearly related to the melting of amphibole and phlogopite (Samples V-706, V-99; Vitim filed, samples B-002, B-012, B-401; Bartoy field). Their origin is similar with glasses discussed recently by Shaw and Klugel (2002). However, origin of some other glasses is obscured. In present paper we would like to discuss some particular problems related to the origin of glasses and melt pocket assemblages. They can be summarized as follows: (1) in situ production of SiO_2-rich (55-57 wt.%) melt by partial melting of peridotite; (2) origin of silicic glasses (SiO_2>70 wt.%) and equilibrium of acid glasses with primary minerals and microlites; (3) formation of microlites including origin of unidentified microlite assemblage (clinopyroxene+olivine+sanidine) in Burkal xenoliths.

1. Majority of glasses observed in mantle xenoliths and in particular in primary/pseudo-secondary melt inclusions in the minerals are Si-rich (typically 51-60 wt.%). Schiano *et al.* (1998) suggested that these glasses can be related to low degree partial melting of peridotite in situ. Kinzler and Langmuir (1995) noticed a discrepancy between experimental data on peridotite melting at 10–15 kbar, when the initial melt (1–2% of partial melting) is SiO_2-rich (up to 57 wt.%, Baker *et al.*, 1995; Robinson *et al.*, 1998), and the composition of natural alkaline basalts undersaturated in SiO_2 (40–45 wt.%). We can suppose that this is due to the differences in melting conditions during the formation of the basaltic magmas and experimental liquids/intergranular melt in xenoliths. Low degree melting of metasomatized mantle in the presence of hydrous fluid, amphibole and/or phlogopite produces SiO_2-undersaturated melts, up to nephelinites and picrites. Minor melting of peridotite in a dry system results in SiO_2-rich melts, which consistent with composition of melt inclusions in minerals. It should be noted that study of intergranular films between mineral grains in natural peridotites, which supposed to represent intermediate state between solid and melt, showed that they contain up to 80 wt.% SiO_2 (Wirth and Franz, 2000). Other important factors are the depth of melt generation and influence of volatiles. At pressures above 10–15 kbar, partial melt of peridotite become SiO_2 undersaturated and correspond to tholeiite, trachybasalt or basanite (Baker and Stolper, 1994; Kinzler and Grove, 1992; Kinzler and Langmuir, 1995). These changes can be related to CO_2 effect. Our data (Simonov *et al.*, 1992) and data by Schiano *et al.* (1998) indicate that H_2O content in the fluid inclusions trapped at

pressures of 10–12 kbar is less than 0.2 wt.%, whereas CO_2 content is typically close to 100%. Solubility of CO_2 in the melt is low at 10 kbar (Blank and Brooker, 1994) and it occurs mainly in molecular form rather than CO_3^{2-}. Therefore, SiO_2 content of the melt can be high in response to accumulation of alkalis in low degree melt (Hirschmann *et al.*, 1998). In contrast, solubility of CO_2 in the melt increase with increasing pressure above 10 kbar (Blank and Brooker, 1994) and CO_3^{2-} ion in the melt form carbonate complexes K_2CO_3, Na_2CO_3 and $CaCO_3$ (Rubie *et al.*, 1983). Therefore, activity of alkalis, a catalyst of SiO_2 accumulation in the melt, decreases (Schiano *et al.*, 1998).

Litasov *et al.* (2003b) studied in details melt inclusions in Dzhilinda peridotites (Vitim field) and found that composition of heated melt inclusions correspond to partial melts of the mantle peridotite at pressures of about 10 kbar. We observed similar glasses in minerals from garnet lherzolite V–896 (Bereya Quarry, Vitim field) where SiO_2 content is lower (Fig.2, Table 4). This is consistent with above statements about CO_2 solubility in the melt and its influence on SiO_2 content and may indicate that these glasses formed during partial melting of garnet-bearing peridotite at pressures above spinel-garnet transition. Both Dzhilinda and Bereya Quarry data are consistent with pressure estimations from associated fluid inclusions (Fig.9A). It is important to note that some glasses in veinlets and melt pockets have similar compositions. Therefore they can be of the same origin. Although the effect of accumulation of microlites should be estimated to obtain the composition of actual melt trapped by xenoliths (e.g. Shaw and Klugel, 2002; Bali *et al.*, 2002) we can follow the conclusion that percolation of melt and fluid prior to intrusion of major mass of magma is the most likely mechanism for the formation of these glasses (Ionov *et al.*, 1994).

2. Origin of the silicic melt in mantle xenoliths is very controversial. Recent experimental study by Shaw *et al.* (1998) indicates that reaction of orthopyroxene with silica-undersaturated melt at ambient pressure results in olivine, clinopyroxene, spinel and intermediate of silicic melt (SiO_2=60–70 wt.%). We also observed the reaction of orthopyroxene = olivine + SiO_2 (melt) in our experiments at 1 atm (Litasov *et al.*, 2000e). Interstitial glasses with SiO_2 content of 60-70 wt.% were observed only in anhydrous depleted harzburgites (Zingrebbe and Foley, 1995; Newmann and Wulff-Pedersen, 1997; Varela *et al.*, 1999). This is consistent with our data. We detected even higher SiO_2 concentrations (up to 74 wt.%) in the glasses presented both in melt inclusions and interstitial space of anhydrous Dzhilinda (Vitim) and Northern Udokan harzburgites.

Although we could explain origin of the silica-rich glasses it is even more difficult to accept observed crystallization of olivine from this kind of melt (e.g. Fig.5E). The equilibrium of magnesium olivine microlites with interstitial melt is confirmed by regular variations in the olivine compositions depending on the composition of glass (Litasov *et al.*, 2003b) and absence of the signs of reaction between olivine microlites and glass. The possibility of the equilibrium relations between SiO_2-rich (up to 65 wt.%) melt and minerals of mantle peridotites was experimentally observed by Draper and Green (1997). They found that liquidus phases of melt containing 61 wt.% SiO_2 and 7–14 wt.% of Na_2O+K_2O in anhydrous or COH-fluid saturated (X_{H2O}=0.5) system are olivine (at pressures below 10 kbar) and orthopyroxene (at higher pressures). While these data could be relevant for majority of glasses in melt pockets in xenoliths, the relations of silicic melt with 70–74 wt.% SiO_2 and olivine microlites remain uncertain.

3. In the previous paragraphs we discussed equilibrium of olivine and silicic glass in

the melt pockets. Typical assemblage of the melt pockets includes olivine, clinopyroxene, Cr-spinel and glass. However, in many cases feldspars or feldspathoids replace glass in this assembly. These assemblies are typical for mantle xenoliths worldwide (e.g. Ionov *et al.*, 1994; Zingrebbe and Foley, 1995; Bali *et al.*, 2002) and are related to xenolith/host interaction. If small amount of melt was impregnated to peridotite in the depth we will have reaction of this melt with peridotite minerals results in Cr- and Mg-rich clinopyroxene (Fig.7, Udokan) and magnesium (Mg#>91) olivine. The Mg# number of microlite minerals and SiO_2 content of the glasses increase with degree of depletion of peridotite. However, if significant amount of melt impregnates peridotite during transport to the surface chemistry of microlites tends to the minerals observed in host basalt groundmass (see trends shown by arrows in Fig.7).

Spinel lherzolites from Bartoy volcanics contain unusual microlite assemblage forming clinopyroxene-olivine-sanidine symplectites (Fig.8). The compositions of clinopyroxene fall away from the compositions of most microlite compositions due to extremely low Al_2O_3 content (Fig.7). Sanidine is also unusual for Burkal xenoliths and host rocks. Oriented symplectite microstructure indicates replacement of certain mineral. However, calculated bulk compositions of the symplectites do not correspond to any mineral observed in mantle xenoliths from basalts (Table 10). From the other hand, influence of melaleucitite melt in the formation of the symplectites should be negligible, because of low total alkalis in the calculated bulks. The low total Al_2O_3 content is indicative for mantle pyroxenes observed in kimberlite xenoliths worldwide. Additionally, deep-seated clinopyroxene can accommodate significant amount of K_2O (e.g. Harlow, 1997). However, MgO and CaO contents are intermediate between clino- and orthopyroxene. Experimental studies of peridotite systems indicate that at pressures above 70 kbar orthopyroxene dissolve to low-Ca clinopyroxene and garnet. Although additional study of the Burkal symplectites is necessary we can suggest that they represent breakdown after K-bearing pyroxene solid solution from deep mantle. Occasionally appearance of ultradeep minerals or their breakdowns in mantle xenoliths was reported previously for non-kimberlite suites (e.g. Collerson *et al.*, 2000; Keshav and Sen, 2001).

10. Conclusions

1. Petrogenesis of various glasses, microlite assemblages and fluid and melt inclusions in minerals of mantle xenoliths from alkaline volcanics of Baikal-Mongolian region is discussed in present paper. Diversity and compositional variations of glasses vary widely and their origin can be addressed to most previously reported hypotheses. Study of fluid inclusions indicates that depth of trapping is usually well correlated with the depth of Moho estimated from seismic and petrological data. Density of CO_2 fluid inclusions indicates minimum pressures of their origin of 10-15 kbar.

2. Glasses from melt inclusions in minerals of Dzhilinda xenoliths (Vitim flied) can represent direct melts formed by in situ partial melting of peridotite at pressures of 10 kbar, the pressure estimated from fluid inclusions, whereas glasses from melt inclusions in minerals of garnet lherzolite of Bereya Quarry (Vitim flied) can represent melts formed at pressures above 15 kbar. SiO_2 content of these glasses (51–57 wt.%) is consistent with experimental data for low-degree partial melting of peridotite. Associated glasses in veinlets and melt pockets have often similar compositions and therefore they

can be of the same origin.

3. Origin of SiO_2-rich (up to 74 wt.%) glasses from harzburgite xenoliths is consistent with experimental study by Shaw *et al.* (1998) indicating that reaction of orthopyroxene with silica-undersaturated melt at ambient pressure results in olivine, clinopyroxene, spinel and intermediate of silicic melt.

4. We described unusual clinopyroxene-olivine-sanidine symplectites in high-temperature spinel lherzolites from Burkal locality. Calculated bulk compositions of the symplectites indicate that they can represent breakdown after K-bearing pyroxene solid solution from deep mantle.

Acknowledgements

Senior author thanks to Y. Ito for help in EPMA and acknowledges a Center for Northeast Asian Studies (CNEAS), Tohoku University and Japanese Society for Promotion of Sciences for Research Fellowships during 1999–2003. This research was supported by Russian Foundation for Basic Research (N97–05–65309). The constructive comments by T.Yoshida were very helpful to improve the quality of the manuscript.

References

Andersen, T. and Neumann, E.-R., 2001
Fluid inclusions in mantle xenoliths, *Lithos*, 55, 301–320.

Ashchepkov, I.V., 1991
Deep-seated xenoliths of the Baikal rift, Nauka, Novosibirsk (in Russian).

Baker, M.B., Hirschmann, M.M., Ghiorso, M.S., and Stolper, E.M. 1995
Compositions of near-solidus peridotite melts from experiments and thermodynamic calculations, *Nature*, 375, 308–311.

Baker, M.B. and Stolper, E.M., 1994
Determining the composition of high-pressure mantle melts using diamond aggregates, *Geochim. Cosmochim.* Acta, 58, 2811–2827.

Bali, E., Szabo, C., Vaselli, O., and Torok, K., 2002
Significance of silicate melt pockets in upper mantle xenoliths from the Bakony-Balaton highland volcanic field, Western Hungary, *Lithos*, 61, 79–102.

Blank, J.G. and Brooker, R.A., 1994
Experimental studies of carbon dioxide in silicate melts: solubility, speciation, and stable carbon isotope behavior, *Rev. Mineral.*, 30, 57–186.

Bottinga, Y. and Richet, P., 1981
High pressure and temperature equation of state and calculation of the thermodynamic propeties of gaseous carbon dioxide, *Amer. Jour. Sci.*, 281, 615–660.

Brey, G.P. and KöTer, T., 1990
Geothermobarometry in four-phase lherzolites II. New thermobarometers, and practical assessment of existing thermobarometers, *Jour. Petrol.*, 31, 1313–1336.

Chazot, G., Menzies, M., and Harte, B., 1996
Silicate glasses in spinel lherzolites from Yemen: origin and chemical composition, *Chem. Geol.*, 134, 159–179.

Collerson, K.D., Hapugoda, S., Kamber, B.S., and Williams, Q., 2000
Rock from the mantle transition zone: majorite-bearing xenoliths from Malaita, Southwest Pacific, *Science*, 288, 1215–1224.

Coltorti, M., Bonadiman, C., Hintin, R.W., Siena, F., and Upton, B.G.J., 1999
Carbonatite metasomatism of the oceanic upper mantle: evidence from clinopyroxenes and glasses in ultramaphic xenoliths of Grande Comore, Indian Ocean, *Jour. Petrol.*, 40, 133-165.

Delvaux, D. Moeys, R., Stapel, G., Petit, C., Levi, K., Miroshnichenko, A., Ruzhich, V., and San'kov, V., 1997
Paleostress reconstructions and geodynamics of the Baikal region, Central Asia, Part II. Cenozoic rifting, *Tectonophys.*, 282: 1-38.

Dobretsov, N.L., Ashchepkov, I.V., Simonov, V.A., and Zhmodik, S.M., 1992
Interaction of the upper mantle rocks with deep-seated fluids and melts in the Baikal rift zone, *Russ. Geol. Geophys.*, 33 (5), 3-21.

Draper, D.S. and Green, T.H., 1997.
P-T phase relations of silicic, alkaline, aluminous mantle-xenolith glasses under anhydrous and C-O-H fluid-saturated conditions, Jour. Petrol., 38, 187-1224.

Ducea, M. and Saleeby, J., 1998
Crustal recycling beneath continental arcs: silica-rich glass inclusions in ultramafic xenoliths from the Sierra Nevada, California, *Earth Planet. Sci. Lett.*, 156, 101-116.

Edgar, A.D., Lloyd, F.E., Forsyth, D.M., and Barnett, R.L., 1989
Origin of glass in upper mantle xenoliths from the Quaternary volcanics of Gees, West Eifel, Germany, *Contrib. Mineral. Petrol.*, 103, 277-286.

Ermakov, N.P. and Dolgov, Y.A., 1979
Thermobarogeochemistry, Nedra, Moscow, (in Russian).

Ertan, I.E. and Leeman, W.P., 1999
Fluid inclusions in mantle and lower crustal xenoliths from the Simcoe volcanic field, Washington, *Earth Planet. Sci. Lett.*, 154, 83-95.

Francis, D.M., 1976
The origin of amphibole in lherzolite xenoliths from Nunivak Island, Alaska, *Jour. Petrol.*, 17, 357-378.

Francis, D.M., 1987
Mantle-melt interaction recorded in spinel lherzolite xenoliths from the Alligator Lake Volcanic Complex, Yukon, Canada, *Jour. Petrol.*, 28, 569-597.

Frey, F.A. and Green, D.H., 1974
The mineralogy, geochemistry and origin og lherzolite inclusions in Victorian basanites, *Geochim. Cosmochim. Acta*, 33, 1023-1059.

Frezzotti, M.L., De Vivo, B. and Clocchiatti, R., 1991
Melt-mineral-fluid interactions in ultramafic nodules from alkaline lavas of Mount Etna (Sicily, Italy) melt and fluid inclusion evidence, *Jour. Volcanol. Geotherm. Res.*, 47, 209-219.

Frezzotti, M.L., Touret, J.L.R., Lustenhouwer, W., and Neumann, E.-R., 1994
Melt and fluid inclusions in dunite xenoliths from La Gomera, Canary Islands: tracking the mantle metasomatic fluids, *Eur. Jour. Mineral.*, 6, 805-817.

Gasparik, T., 1984
Two-pyroxene thermobarometry with new experimental data in the system CaO-MgO-Al_2O_3-SiO_2, *Contrib. Mineral. Petrol.*, 87, 87-97.

Grachev, A.F., 1998
The Khamar-Daban ridge as a hot spot of the Baikal rift from data of chemical

geodynamics, *Physics of the Solid Earth*, 34, 175–200.

Green, D.H. and Fallon, T., 1998
Pyrolite: A Ringwood concept and its current expression, In Jackson, I. Ed., The *Earth's Mantle, Composition, structure, and evolution*, Cambridge Univ. Press, 311–378.

Griffin, W.L., Wass, S.Y. and Hollis, J.D., 1984
Ultramafic xenoliths from Bullenmerri and Gnotuk maars, Victoria, Australia: Petrology of a subcontinental crust-mantle transition, *Jour. Petrol.*, 25, 53–87.

Harlow, G.E., 1997
K in clinopyroxene at high pressure and high temperature: an experimental study, *Amer. Mineral.*, 82, 259–269.

Herzberg, C.T., 1978
Pyroxene geothermometry and geobarometry: experimental and thermodynamic evaluation of some subsolidus phase relations involving pyroxenes in the system CaO-MgO-Al_2O_3-SiO_2, *Geochim. Cosmochim. Acta*, 42, 945–957.

Hirschmann, M.M., Baker, M.B., and Stolper, E.M., 1998
The effect of alkalis on the silica content of mantle-derived melts, *Geochim. Cosmochim. Acta*, 1998, 62, 883–902.

Holloway, J.R., 1981
Composition and volumes of supercritical fluids in the earth's crust. In: Hollister, L.S., Crawford, M.L. eds. *Fluid Inclusions: Applications to petrology*, Min. Assoc. Canada, Short Course Handbook, v.6, pp.13–38.

Ionov, D.A., Ashchepkov, I.V., Stosch, H.-G., Witt-Eickschen, G. and Seck H.A., 1993
Garnet peridotite xenolith from the Vitim volcanic field, Baikal region: the nature of the garnet-spinel peridotite transition zone in the continental mantle, *Jour. Petrol.*, 34, 1141–1175.

Ionov, D.A., Hofmann, A.W., and Shimizu, N., 1994
Metasomatism-indused melting in mantle xenoliths from Mongolia, *Jour. Petrol.*, 1994, 35, 753–785.

Ionov, D.A., O'Reilly, S.Y., and Ashchepkov, I.V., 1995
Feldspar-bearing lherzolite xenolith in alkali basalts from Hamar-Daban, southern Baikal region, Russia, *Contrib. Mineral. Petrol.*, 118, 131–148.

Keshav, S., and Sen, G., 2001
Majoritic garnet in Hawaiian xenoliths: preliminary results, *Geophys. Res. Lett.*, 28, 3509–3512.

Kinzler, R.J. and Grove, T.L., 1992. Primary magmas of mid-ocean ridge basalts 1. Experiments and methods, *Jour. Geophys. Res.*, 97, 6885–6906.

Kinzler, R.J. and Langmuir, C.H., 1995
Minute mantle melt, *Nature*, 375, 274–275.

Klügel, A., 1998
Reactions between mantle xenoliths and host magma beneath La Palma (Canary Islands): constraints on magma ascent rates and crustal reservoirs, *Contrib. Mineral. Petrol.*, 131, 237–257.

LeMaitre, R.W., 1989
A classification of igneous rocks and glossary of terms, Oxford, Blackwell.

Litasov, K.D., Fujimaki, H., Miyamoto, T., Taniguchi, H., 1999a

Glasses in mantle xenoliths from Miocene picrobasalts of the Vitim volcanic field, Baikal region, Russia. *Abst. Vol. of Ann. Meeting of Japanese Soc. of Mineral., Petrol. and Econ. Geol.*, Ibaraki Univ., Mito, Japan, p.214.

Litasov K.D., Rasskazov S.V., Ivanov A.V., 1999b
Depleted and enriched spinel peridotites in xenoliths from the Late Cenozoic basanite, Lake Kuas area, Udokan Ridge, East Siberia, *Transact. (Doklady) Rus. Acad. Sci., Earth Sci. Sect.*, 369 (8), 1156-1160.

Litasov, K.D. and Litasov, Yu.D., 1999
Petrology of garnet-spinel lherzolites and accompanying xenoliths from Pliocene-Pleistocene basanites of the Vitim volcanic plateau, *Russ. Geol. Geophys.*, 40, 546–558.

Litasov, K.D., Litasov, Y.D., Mekhonoshin, A.S., and Mal' kovets, V.G., 2000a
Mineralogy of mantle xenoliths from Pliocene basanites of the Dzhilinda River (Vitim volcanic field). *Russ. Geol. Geophys.*, 41, 1532–1554.

Litasov, K.D., Litasov, Y.D., Mekhonoshin, A.S., and Mal' kovets, V.G., 2000b
Geochemistry of clinopyroxenes and petrogenesis of mantle xenoliths from Pliocene basanites of the Dzhilinda River (Vitim volcanic field), *Russ. Geol. Geophys.*, 41, 1555–1572.

Litasov, K.D., Foley, S.F., and Litasov, Yu.D., 2000c
Magmatic modification and metasomatism of the subcontinental mantle beneath the Vitim volcanic field (East Siberia): evidence from trace element data on pyroxenite and peridotite xenoliths from Miocene picrobasalt, *Lithos*, 54, 83–114.

Litasov, K.D., Ito, Y., Litasov, Y.D., Kitakaze, A., Taniguchi, H., and Ohtani, E., 2000d
New Data on Xenoliths and Megacrysts from Alkaline Basalts of Bartoy Volcanic Field (Baikal Region, Russia). *Northeast Asian Studies*, 5, 113–147.

Litasov, K., Ohtani, E., Simonov, V., and Taniguchi, H., 2000e
Melting experiments on the mantle minerals and basaltic melts: possible relation to the melt-xenolith reactions during magma ascent. *Abst. Vol. 32th Int. Geol. Congr.*, Rio de Janeiro, Brazil, CD-edition.

Litasov K.D., Ito Y., Malkovets V.G., Litasov Yu.D., Taniguchi H., 2002
Primary mineralogy of Late Miocene picrobasalt from Vitim volcanic field: evidences for xenolith/host interaction. *Northeast Asian Studies*, 7: 191-203.

Litasov K.D., Taniguchi H., 2002
Mantle evolution beneath Baikal rift. Center for Northeast Asian Studies, Tohoku University, Japan, CNEAS Monograph Series, v.5.

Litasov, K.D., Simonov, V.A., Sharygin, V.V., Kovyazin, S.V., Malkovets, V.G., and Litasov, Y.D., 2003a
Fluids and glasses in mantle xenoliths from Vitim volcanic field: evidences for in situ partial melting and xenolith/host interaction. *Abst. Eur. Union Geosci. 12, Geophys. Res. Abst.*, v.5, p.04827.

Litasov, K.D., Simonov, V.A., Kovyazin, S.V., Litasov, Yu.D., and Sharygin, V.V., 2003b
Interaction between mantle xenoliths and deep-seated melts: results of study of melt inclusions and interstitial glasses in peridotites from basanites of the Vitim volcanic field. *Russ. Geol. Geophys.*, 44, 436–450.

Logatchev, N.A., 1993
History and geodynamics of the Baikal rift (east Siberia): a review. *Bull. Centr. Rech.*

Explor. Prod. Elf Aquitaine, 17 (2), 353–370.

Murck, B.W., Burruss, R.C. and Hollister, L.S., 1978
Phase equilibria in fluid inclusions in ultramafic xenoliths. *Amer. Miner.* 63, 40–46.

Neumann, E.-R. and Wuiff-Pedersen, E., 1997
The origin of highly silicic glass in mantle xenoliths from the Canary Island, *Jour. Petrol.*, 38, 1513–1539.

O'Neill, H.St.C., 1981
The transition between spinel lherzolite and garnet lherzolite, and its use as geobarometer, *Contrib. Mineral. Petrol.*, 77, 185–194.

Olafsson, M. and Eggler, D.H., 1983
Phase relations of amphibole, amphibole-carbonate, and phlogopite-carbonate peridotite: petrologic constraints on the asthenosphere, *Earth Planet.Sci. Lett.*, 64, 305–315.

O'Reilly, S.Y. and Griffin, W.L., 1985
A xenolith-derived geotherm for Southeastern Australia and its geophysical implications, *Tectonophys.*, 111, 41–63.

Press, S., Witt, G., Seck, H.A., Ionov, D.A., and Kovalenko, V.I., 1986
Spinel peridotite xenoliths from the Taryat depression, Mongolia I: Mayor element chemistry and mineralogy of a primitive mantle xenolith suite, *Geochim. Cosmochim. Acta*, 50, 2587–2599.

Rasskazov, S.V., 1994
Magmatism related to the Eastern Siberia rift system and the geodynamics, *Bull. Centres Rech. Explor.-Prod. Elf Aquitaine*, 18 (2), 437–452.

Rasskazov, S.V., Ivanov, A.V., Bogdanov, G.V., and Medvedeva, T.V., 1994
The composition of orthopyroxene and systematization of deep-seated inclusions from volcanic rocks of Oka and Tunka regions of the Baikal rift system, *Transact. (Doklady) Russ. Acad. Sci.*, 338 (5), 649–654.

Rasskazov, S.V., 1993
Magmatism of Baikal rift system, Nauka, Novosibirsk (in Russian).

Rasskazov, S.V., Boven, A., Andre, L., Liejua, J.-P., Ivanov, A.V., and Punzalan, L., 1997
Evolution of magmatism in Northeast Baikal rift system, *Petrology*, 5, 115–136.

Robinson, J.A.C., Wood, B.J., and Blundy, J.D., 1998
The begining of melting of fertile and depleted peridotite at 1.5 GPa, *Earth Planet. Sci. Lett.*, 155, 97–111.

Roedder, E., 1965
Liquid CO_2 inclusions in olivine-bearing nodules and phenocrysts from basalts, *Amer. Mineral.*, 50, 1746–1782.

Roedder, E., 1984
Fluid Inclusions, Mineral. Soc. Amer., Rev. Mineral., 12.

Rubie, D.C. and Gunter, W.D., 1983
The role of speciation in alkaline igneous fluids during fenite metasomatism, *Contrib. Mineral. Petrol.*, 82, 165–175.

Schiano, P. and Clocchiatti, R., 1994
Worldwide occurrence of silica-rich melts in sub-continental and sub-oceanic mantle minerals, *Nature*, 368, 621–624.

Schiano, P., Clocchiatti, R., Shimizu, N., Weis, D. and Mattielli, N., 1994

Cogenetic silica-rich and carbonate-rich melts trapped in mantle minerals in Kerguelen ultramafic xenoliths: implications for metasomatism in the oceanic upper mantle, *Earth Planet. Sci. Lett.*, 123, 167–178.

Schiano, P., Clocchiatti, R., Shimizu, N., Maury, R.C., Jochum, K.P., and Hofmann, A.W., 1995
Hydrous silica-rich melts in the sub-arc mantle and their relationship with erupted arc lavas, *Nature*, 377, 595–600.

Schiano, P., Bourdon, B., Clocchiatti, R., Massare, D., Varela, M.E., Bottinga, Y., 1998
Low-degree partial melting trends recorded in upper mantle minerals, *Earth Planet. Sci. Lett.*, 160, 537–550.

Schiano, P., Clocchiatti, R., Bourdon, B., Burton, K., and Thellier, B., 2000
The composition of low-degree partial melts at the garnet-spinel transition zone, *Earth Planet. Sci. Lett.*, 174, 375–383.

Sharygin, V.V., Litasov, K.D., Smirnov, S.Z., Kuzmin, D.V., Reutsky, V.N., and Ivanov, A.V., 1998
Fluid and Silicate-Melt Inclusions and Interstitial Glass in Mantle Xenoliths from Melanephelinites of the Udokan Lava Plateau, Russia, *Ext. Abst. 7th Int. Kimb. Conf.*, Cape Town, South Africa, pp.791–793.

Shaw, C.S.J., Thibault, Y., Edgar, A.D., and Lloyd, F.E., 1998
Mechanisms of orthopyroxene dissolution in silica-undersaturated melts at 1 atmosphere and implications for the origin of silica-rich glass in mantle xenoliths, *Contrib. Mineral. Petrol.*, 132, 354–370.

Shaw, C.S.J. and Klugel, A., 2002
The pressure and temperature conditions and timing of glass formation in mantle derived xenoliths from Baarley, West Eifel, Germany: the case for amphibole breakdown, lava infiltration and mineral-melt reaction, *Mineral. Petrol.*, 74, 163–187.

Simonov, V.A., 1993
Petrogenesis of ofiolites (thermobarogeochemistry study). UIGGM Press, Novosibirsk (in Russian).

Simonov, V.A., Stolpovskaya, V.N., and Ashchepkov, I.V., 1992
Pecularities of chromatography analysis of the volatile components of the mantle xenoliths and magmatic glasses. *In: Thermobarogeochemistry of rock-forming processes*, UIGGM Press, Novosibirsk, v.2, pp.48–54 (in Russian).

Sobolev, A.V. and Slutsky, A.B., 1984
Composition and condition of crystallization for primary melts of Siberian meimechites and origin of ultramafic magmas, *Russ. Geol. Geophys.*, 25 (12), 97–110.

Solovova, I.P., Ryabchikov, I.D., Kovalenko, V.I., and Naumov, V.B., 1982
Inclusions of dense CO_2 in mantle lnerzolites, *Trans. (Doklady) Akad. Sci. USSR*, 263, 179–182.

Spera, F.J. and Bergman, S.C., 1980
Carbon dioxide in igneous petrogenesis I. Aspects of the dissolution of CO_2 in silicate liquids. *Contrib. Mineral. Petrol.*, 74, 55–66.

Stupak, F.M., 1987
Cenozoic volcanism of the Udokan ridge, Nauka, Novosibirsk (in Russian).

Szabo C. and Bodnar R.J., 1996

Changing magma ascent rates in the Nograd-Gomor volcanic field Northern Hungary/Northern Slovakia: Evidence from CO_2-rich fluid inclusions in metasomatized upper mantle xenoliths, *Petrology*, 4, 240–249.

Szabo, C., Bodnar, R.J., and Sobolev, A.V., 1996
Metasomatism assotiated with subduction-related, volatile-rich silicate melt in the upper mantle beneath the Nograd-Gomor Volcanic field, Norhtern Hungary/Southern Slovakia: Evidence from silicate melt inclusions, *Eur. Jour. Mineral.*, 8, 881–899.

Takahashi, E. and Kushiro, I., 1983
Melting of a dry peridotite at high pressures and basalt magma genesis, *Amer. Mineral.*, 68, 859–879.

Varela, M.E., Clocchiatti, R., Kurat, G., Schianom P., 1999
Silicic glasses in hydrous and unhydrous mantle xenoliths from Western Victoria, Australia: at least two different sources, *Chem. Geol.*, 153, 151–169.

Wallace, M.E. and Green, D.H., 1991
The effect of bulk rock composition on the stability of amphibole in the upper mantle: implications for solidus positions and mantle metasomatism, *Mineral. Petrol.*, 44, 1–19.

Wirth, R. and Franz, L., 2000
Thin amorphous intergranular layer at mineral interfaces in xenoliths: the early stage of melting, In: Bagdassarov, N., Laporte, D., and Thompson, A.B. eds., *Physics and chemistry of partially molten rocks*, Kluwer Acad. Publ., Dordrecht, Netherlands, Petrology and Structural Geol. Ser., 2000, v.11, pp.229–268.

Wullf-Pedersen, E., Neumann, E.-R., and Jensen, B.B., 1996
The upper mantle under La Palma, Canary Island: formation of Si-K-Na-rich melt and its importance as a metasomatic agent, *Contrib. Mineral. Petrol.*, 125, 113–139.

Wullf-Pedersen, E., Newmann, E.-R., Vannucci, R., Bottazzi, P., and Ottolini, L., 1999
Silicic melts produced by reaction between peridotite and infiltrating basaltic melts: ion probe data on glasses and minerals in veined xenoliths from La Palma, Canary Island, *Contrib. Mineral. Petrol.*, 137, 59–82.

Wyllie, P.J., 1978
Mantle fluid compositions buffered in peridotite-CO_2-H_2O by carbonates, amphibole, and phlogopite, *Jour. Geol.*, 86, 687–713

Xu, Y., Mercier, J.-C.C., Lin, Y., Shi, L., Menzies, M.A., Ross, J.V., Harte, B., 1996
K-rich glass-bearing wehrlite xenoliths from Yitong, Northeastern China: petrological and chemical evidence for mantle metasomatism, *Contrib. Mineral. Petrol.*, 125, 406–420.

Yarmolyuk, V.V. and Kovalenko, V.I., 1990
South-Baikal "hot spot" and its role in formation of the Baikal rift system, *Transact. (Doklady) Russ. Acad. Sci.*, 312 (1), 187–191.

Yaxley, G.M. and Kamenetsky, V., 1997
In situ origin for glass in mantle xenoliths from southeastern Australia: insight from trace element compositions of glasses and metasomatic phases, *Earth Planet. Sci. Lett.*, 1997, 172, 97–109.

Zinngrebe, E. and Foley, S.F., 1995
Metasomatism in mantle xenoliths from Gees, West Eifel, Germany: evidence for

the genesis of calc-alkaline glasses and metasomatic Ca-enrichment, *Contrib. Mineral. Petrol.*, 122, 79–96.

Zorin, Y.A., Kozhevnikov, V.M., Novoselova, M.R., and Turutanov, E.H., 1989 Thickness of the lithosphere beneath the Baikal rift zone and adjacent regions, *Tectonophys.*, 168, 327–337.